Decarbonizing copper production by power-to-hydrogen: A techno-economic analysis

Journal Article

Author(s):
Röben, Fritz T.C.; Schöne, Nikolas; Bau, Uwe; Reuter, Markus A.; Dahmen, Manuel; Bardow, André (iD)
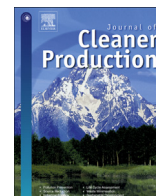
Decarbonizing copper production by power-to-hydrogen: A techno-economic analysis

Fritz T.C. Röben [a, b], Nikolas Schöne [a], Uwe Bau [a], Markus A. Reuter [c, d], Manuel Dahmen [a], André Bardow [e, a, f, g, *]

[a] *Institute of Energy and Climate Research - Energy Systems Engineering (IEK-10), Forschungszentrum Jülich GmbH, 52425, Jülich, Germany*
[b] *RWTH Aachen University, 52062, Aachen, Germany*
[c] *SMS Group GmbH, 40237, Düsseldorf, Germany*
[d] *Helmholtz Institute Freiberg for Resource Technology (HIF), 09599, Freiberg, Germany*
[e] *JARA-ENERGY, 52425, Jülich, Germany*
[f] *Institute of Technical Thermodynamics, RWTH Aachen University, 52062, Aachen, Germany*
[g] *Energy & Process Systems Engineering, ETH Zürich, 8092, Zürich, Switzerland*

ABSTRACT

Electrifying energy-intensive processes is currently intensively explored to cut greenhouse gas (GHG) emissions through renewable electricity. Electrification is particularly challenging if fossil resources are not only used for energy supply but also as feedstock. Copper production is such an energy-intensive process consuming large quantities of fossil fuels both as reducing agent and as energy supply.

Here, we explore the techno-economic potential of Power-to-Hydrogen to decarbonize copper production. To determine the minimal cost of an on-site retrofit with Power-to-Hydrogen technology, we formulate and solve a mixed-integer linear program for the integrated system. Under current techno-economic parameters for Germany, the resulting direct CO_2 abatement cost is 201 EUR/t CO_2-eq for Power-to-Hydrogen in copper production. On-site utilization of the electrolysis by-product oxygen has a substantial economic benefit. While the abatement cost vastly exceeds current European emission certificate prices, a sensitivity analysis shows that projected future developments in Power-to-Hydrogen technologies can greatly reduce the direct CO_2 abatement cost to 54 EUR/t CO_2-eq. An analysis of the total GHG emissions shows that decarbonization through Power-to-Hydrogen reduces the global GHG emissions only if the emission factor of the electricity supply lies below 160 g CO_2-eq/kWh$_{el}$.

The results suggest that decarbonization of copper production by Power-to-Hydrogen could become economically and environmentally beneficial over the next decades due to cheaper and more efficient Power-to-Hydrogen technology, rising GHG emission certificate prices, and further decarbonization of the electricity supply.

© 2021 The Authors. Published by Elsevier Ltd. This is an open access article under the CC BY license (http://creativecommons.org/licenses/by/4.0/).

1. Introduction

The reduction of CO_2 emissions in the industrial sector will be crucial to meet the goals for climate change mitigation (Rogelj et al., 2018; de Coninck et al., 2018). Besides increased energy efficiency, additional options are necessary to reduce emissions (Fischedick et al., 2014b). An increasingly powerful tool for reducing emissions is electrification due to the rapid decarbonization of power supply (Luderer et al., 2018).

However, replacing fossil fuels with electricity is not always directly possible since fossil fuels serve two use cases in energy-intensive industries: 1) the supply of process heat by combustion and 2) the use as chemical feedstock. Process heat demand is typically large and only few alternatives to fossil fuels can supply heat at the required consistency, fluxes, and in particular high temperatures (Friedmann et al., 2019). A promising alternative to fossil fuels is the combustion of renewable hydrogen (H_2) to provide high-temperature process heat (Friedmann et al., 2019). Renewable H_2 can often also be used as an alternative chemical feedstock.

Nomenclature

Abbreviations

AEL	Alkaline electrolysis
AF	Anode furnace
ASU	Air separation unit
C	Carbon
CH_4	Methane
CO_2-eq	Carbon dioxide equivalent
EL	Electrolyzer system
GHG	Greenhouse gas
H_2	Hydrogen
H2C	Hydrogen compressor
H2st	Hydrogen storage
MILP	Mixed-integer linear program
O_2	Oxygen
PEMEL	Polymer electrolyte membrane electrolysis
PES	Process electricity supply
PHS	Process heat supply
SCF	Slag-cleaning furnace
SOEL	Solid oxide electrolysis
TAC	Total annualized cost
VL	Valve
WACC	Weighted average cost of capital

Sets

$c \in \mathscr{C}$	Components = {EL, H2st, H2C, VL, PHS, AF, SCF, PES}
$d \in \mathscr{D}$	Demands = {phd, O2d, rad, rsd, phsd, eld}
$i \in \mathscr{I}$	Intermediates = {H2, pH2, O2e}
$s \in \mathscr{S}$	Sources = {el, CH4, C, O2s}
$t \in \mathscr{T}$	Time steps

Parameters

α	CO_2 cap in relation to conventional operation [-]
Δh_R	Enthalpy of reaction [kJ/mol]
$\dot{D}_{d,t}$	Time-specific process demands [kW, kg/h]
$\varepsilon_{s,c}^{dir}$	Direct CO_2 emission factors [g/kWh]
ε_s^{ind}	Indirect GHG emission factors [g/kWh]
η_{c,e_o,e_i}	Efficiency of component [-, kg_{O2}/kWh_{H2}]
$\nu_{c,\Delta e_o,H2}$	Correction factor for H_2 use [-]
CO_2^{AL}	Annual limit of direct CO_2 emissions [g/a]
CO_2^{conv}	Conventional CO_2 emissions [g/a]
cpx_c^{fix}	Fixed investment costs [EUR]
cpx_c^{var}	Size-specific investment costs [EUR/kW]
CRF	Capital recovery factor [1/a]
int	Interest rate of investment [%]
n	Lifetime of the project [a]
n_{stk}	Lifetime electrolyzer stack [a]
o_c^{min}	Minimal part-load factor [-]

opx_c^{fix}	Fixed annual operation and maintenance cost factor [%/a]
P_c^{max}	Maximal installation size [kW]
P_c^{min}	Minimal installation size [kW]
$p_{s,t}$	Commodity prices [EUR/kWh, EUR/kg]
LHV_s	Lower heating value [kWh/mol]

Variables

$\dot{E}_{e,c,t}$	Energy/material flow $e \in \mathscr{S} \cup \mathscr{I} \cup \mathscr{D}$ [kW, kg/h]
$\dot{S}_{s,t}$	Supply of energy/material [kW, kg/h]
CO_2^{dir}	Time-specific direct CO_2 emissions [g/h]
CO_2^{dir}	Annual direct CO_2 emissions [g/a]
CPX_c	Capital expenditures [EUR]
GHG^{ind}	Annual indirect GHG emissions [g/a]
GHG^{tot}	Annual total GHG emissions [g/a]
OPX_c^{fix}	Fixed annual operation and maintenance costs [EUR/a]
$OPX_{s,t}^{var}$	Variable operating costs [EUR/h]
P_c^N	Capacity of component [kW]
$P_{c,t}^O$	Operation rate of component [kW]
SOC_0	Initial state of charge of the H_2 storage [kWh]
SOC_t	State of charge of the H_2 storage [kWh]
$x_{c,t}$	Decision to operate component [-]
y_c	Decision to install component [-]

Subscripts

$\Delta phd, H2$	Process heat demand savings when using H_2 as reducing agent
$\Delta phsd, H2$	Process heat demand savings in SCF when using H_2 as reducing agent
e_i	Material/energy input
e_o	Material/energy output
stk	Electrolyzer stack
el	electricity
eld	electricity demand
O2d	Oxygen demand
O2e	Oxygen from water electrolysis
O2s	Oxygen source
pH2	Pressurized hydrogen
phd	Process heat demand
phsd	Process heat demand SCF
rad	Reducing agent demand AF
rsd	Reducing agent demand SCF

Superscripts

dir	Direct
fix	Fixed
ind	Indirect
tot	Total
var	Variable

Water electrolysis systems can produce H_2 from water and renewable electricity and thus are often summarized under the term Power-to-H_2. These systems are already commercially available at large system sizes of several MW power rating (Siemens AG, 2018). Additionally, further improvements are expected with regard to technical and economic performance (Buttler and Spliethoff, 2018). Due to these attractive features, Power-to-H_2 systems are intensively investigated in literature (Parra et al., 2019) and in numerous demonstration projects around the world (Thema et al., 2019).

A prominent example for H_2 as a decarbonization option for energy-intensive industries is steel production (Fischedick et al., 2014a; Weigel et al., 2016; Otto et al., 2017; Thyssenkrupp, 2019). Studies show that steel production with direct hydrogen reduction is economically and environmentally the most promising processing route (Fischedick et al., 2014a; Weigel et al., 2016). In practice, Thyssenkrupp, a large steel producer, recently started injecting hydrogen as reducing agent into a blast furnace (Thyssenkrupp, 2019). In addition to their use as reducing agents, fossil fuels are currently required for the provision of process heat. Here, the

combustion of synthetic natural gas produced by methanation of renewable H_2 and carbon-rich off-gases, e.g., from steel production, represents a further decarbonization option in integrated steel plants (Rosenfeld et al., 2020).

Hydrogen could take a similar role in the energy-intensive production of copper. Reducing copper production's environmental impact is important as the global copper demand is expected to triple from 2010 to 2050 (Elshkaki et al., 2016). This strong increase in global copper demand is mostly attributed to socio-economic development (Elshkaki et al., 2016; Deetman et al., 2018; Henckens and Worrell, 2020). A significant driver for growth is due to the fact that copper is a key element for low-carbon technologies like renewable electricity and electric vehicles and thus a central material for a sustainable energy transition (Deetman et al., 2018; Kuipers et al., 2018). The specific climate change impact per copper produced is expected to decrease due to a cleaner electricity supply. However, this decrease can only partially compensate for the additional emissions due to higher copper demand (Kuipers et al., 2018). Consequently, several studies consistently forecast that copper production's climate change impact will significantly increase if no additional measures are taken (Van der Voet et al., 2018; Kuipers et al., 2018; Dong et al., 2020).

Copper's mass-specific climate impact is three times higher than for iron (Van der Voet et al., 2018). Accordingly, several recent studies analyze the life-cycle of copper with a focus on the impact of mines (Song et al., 2017; Segura-Salazar et al., 2019), primary production technologies (Kulczycka et al., 2016), and the recycling of copper-rich waste (Zhang et al., 2021) for a circular economy (Soulier et al., 2018; Bonnin et al., 2019; Reuter et al., 2015, 2019). The reported climate change impact of copper production ranges from 1.1 to 8.9 kg CO_2-eq per kg of refined copper (Dong et al., 2020). The wide variation of environmental impacts is due to different production technologies, ore grades, and local energy mixes (Dong et al., 2020), especially at the location of the mine (Abadías Llamas et al., 2019). The climate change impact, in particular, is strongly linked to energy consumption (Kuipers et al., 2018). Thus, a clean energy supply is important to reduce copper production's impact (Dong et al., 2020), particularly to mitigate the rising energy demand due to the general decline of copper ore grades at the mining sites. The energy-focused analysis by Moreno-Leiva et al. (2019) concluded that detailed assessment and optimal design of energy systems in copper production can enable economic and environmental benefits, with the integration of renewable energy supply offering a large potential. However, the direct use of low-carbon electricity only reduces greenhouse gas (GHG) emissions related to electricity consumption, while emissions remain from process-related use of fossil fuels. To further reduce the climate impact, production systems need to employ clean fuels across the production chain of copper (Dong et al., 2020). Power-to-H_2 provides a potential pathway to also eliminate process-related emissions. So far, the integration of Power-to-H_2 both in the energy supply system and the production process has not been analyzed, despite the importance of copper and the promising application due to the co-utilization of oxygen.

First tests on the use of H_2 in copper production were recently carried out, identifying promising applications in hydrogen burners, anode refining furnaces, and melting units (Degel et al., 2019). H_2 has also successfully been employed experimentally as an alternative reducing agent (Goyal et al., 1982; Parra De Lazzari and Capocchi, 1997; Marin and Utigard, 2010; Qu et al., 2020). As copper production also requires oxygen, on-site integration of a Power-to-H_2 system becomes particularly attractive, as the electrolysis by-product O_2 can partially replace its current supply by energy-intensive cryogenic air separation.

To evaluate the environmental and economic potential of retrofitting copper production with a Power-to-H_2 system, a detailed model is necessary for the integrated supply system for energy and materials. Although the potential of Power-to-H_2 systems has been analyzed for many applications (Bertuccioli et al., 2014; Brunner et al., 2015; Parra et al., 2017; van Leeuwen and Mulder, 2018; Nguyen et al., 2019; Morgenthaler et al., 2020), the integration with co-utilization of O_2 and H_2 has not yet been investigated for copper production.

In this contribution, our main objective is to determine the techno-economic potential of decarbonizing copper production by Power-to-H_2 technology. The techno-economic potential is quantified by the minimal abatement cost of direct CO_2 emissions. To also evaluate the overall climate change impact, we assess the total greenhouse gas emissions, including upstream processes, e.g., electricity supply. For this purpose, an optimal system design is proposed for a representative copper production site. A model is developed for the energy supply system for copper production integrating a Power-to-H_2 system. Through numerical optimization, this model is used to analyze the techno-economic potential of decarbonizing copper production. Specifically, we formulate and solve a mixed-integer linear program (MILP) that minimizes the total annualized cost (TAC), varying GHG emissions reductions. As several parameters such as investment cost and efficiency of the water electrolyzer in Power-to-H_2 systems are expected to change in the future, we conduct a broad sensitivity analysis to give an outlook on the future economic and environmental impacts.

The remainder of the paper is structured as follows: Section 2 gives a brief overview of copper production, Power-to-H_2 technology and states the assumptions and parameters used in our analysis. Section 3 presents the mixed-integer linear program. In Section 4, the results of the optimization and sensitivity analysis are presented. Finally, conclusions are drawn in Section 5.

2. Material and data: Retrofitting copper production with Power-to-H_2

In this section, we give an overview of the reference copper production plant and a Power-to-H_2 system. Section 2.1 provides a brief overview of the conventional reference process. In Section 2.2, we discuss the assumptions and parameters for the use of H_2 and O_2 in the process. Technical and economic parameters of the Power-to-H_2 system are presented in Section 2.3. Indirect GHG emissions from upstream processes are examined in Section 2.4. Section 2.5 details the assumptions with respect to commodity prices and energy demand profiles.

2.1. Conventional copper production

The production of copper consists of several process steps to produce highly pure copper from copper concentrate. Our reference production process is based on Schlesinger et al. (2011) and its retrofit with Power-to-H_2 technology is shown in Fig. 1.

In the flash furnace, copper concentrate is smelted into a molten mass. The required energy originates from oxidizing iron and sulfides in the concentrate. The oxidation takes place in an oxygen-enriched blast of 50−70% O_2, thus requiring large quantities of O_2. In the furnace bath, the molten mass separates into two layers with copper-rich matte (50−70 wt-% Cu) at the bottom and lighter slag, containing mostly iron oxides, at the top. Matte is sent to the converters and slag to the slag-cleaning furnace. The slag-cleaning furnace recovers matte droplets entrapped in the slag. To enhance recovery and maintain a low-viscosity slag, the slag is kept at operating temperature and a layer of coke acts as reducing agent. Recovered matte is added to the converters along with matte from
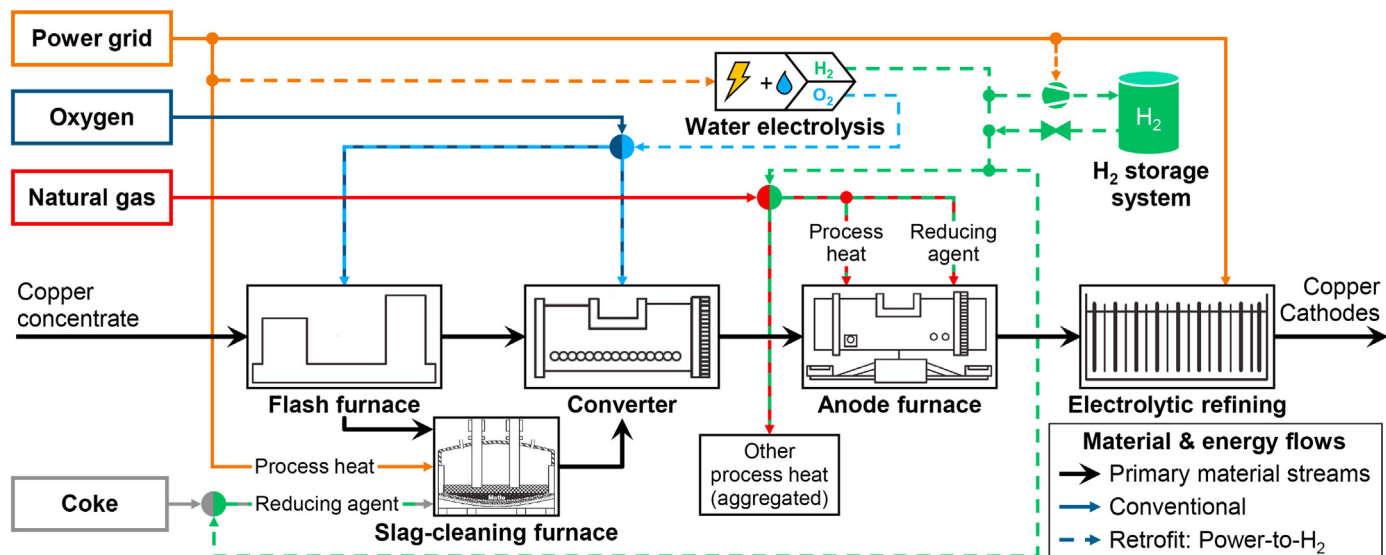
Fig. 1. Flowsheet of copper production process retrofitted with Power-to-H₂ technology to supply hydrogen as reducing agent in the anode furnace and slag-cleaning furnace, and to supply high-temperature process heat. The electrolysis by-product oxygen is utilized in the flash furnace and converters. The structure of the conventional copper production process is based on Schlesinger et al. (2011) and represented by solid lines, while the new material streams for the Power-to-H₂ system are represented by dashed lines. The other process heat (aggregated) represents the further process heat demands in the plant besides those explicitly mentioned.

flash smelting. In the converters, oxygen-enriched air (22−28 vol-% O_2) is blown through the matte to oxidize iron and sulfides and produce blister copper of 99 wt-% copper. The blister copper is sent to the anode furnaces where remaining sulfur and oxygen are removed by blowing first air and then a reducing agent through the melt. Typically, natural gas is used as reducing agent, but other fossil fuels are also in use (Ramachandran et al., 2003). The resulting melt has a purity of 99.5 wt-% copper and is cast into copper anodes. The anodes are electrolytically refined to copper cathodes of 99.99 wt-% purity in the final process step. The corresponding energy demands of an exemplary copper production plant are shown in Table 1 (Aurubis, 2019).

Copper production processes are very heterogeneous due to different geological, geographical, and technological conditions (Kuipers et al., 2018). However, the chosen reference process applies the most commonly used technologies for smelting and converting, i.e., flash smelting and Peirce-Smith converting (Wang et al., 2019). Further, virtually all molten copper is fire refined and electrolytically refined (Schlesinger et al., 2011), as performed in our reference process. Thus, our reference process reflects the most common setup of copper production and should therefore be representative to establish the techno-economic potential of Power-to-H₂. The carbon footprint of copper produced by the reference plant corresponds to a comparatively low value in relation to other reported copper productions (Dong et al., 2020), which strongly depends on the specific impacts of mining operations

(Abadías Llamas et al., 2019), but also indicates rather high efficiency of the analyzed process. Thus, the considered plant rather corresponds to a challenging case for decarbonization of copper.
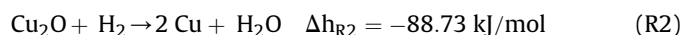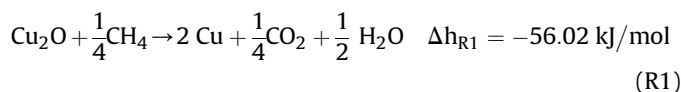
2.2. Copper production with Power-to-H₂ and −O₂

The considered integration of a Power-to-H₂ system into copper production is shown in Fig. 1. In the following, we discuss our assumptions for the use of H₂ and O₂ in copper production.

2.2.1. H₂ as reducing agent in anode furnaces

Different copper production plants use different reducing agents to deoxidize the molten blister copper (Ramachandran et al., 2003). In our reference process, natural gas (CH_4) is used as reducing agent (Schlesinger et al., 2011). While there is little public information about the industrial practice of using H₂ instead of CH_4 in anode furnaces, experimental investigations have shown that H₂ is an effective reducing agent for refining molten copper (Goyal et al., 1982; Parra De Lazzari and Capocchi, 1997; Marin and Utigard, 2010).

Due to a lack of public data, we assume that the reducing agents CH_4 and H₂ react completely in the melt. Note that utilization in industrial practice is typically not complete and will likely differ between CH_4 and H₂ due to differing transport phenomena at the interface between gas and liquid metal. To estimate the theoretical potential of replacing CH_4 by H₂, we consider complete conversion in the two reactions:

$$Cu_2O + \frac{1}{4}CH_4 \rightarrow 2\,Cu + \frac{1}{4}CO_2 + \frac{1}{2}\,H_2O \quad \Delta h_{R1} = -56.02 \text{ kJ/mol}$$
(R1)

$$Cu_2O + H_2 \rightarrow 2\,Cu + H_2O \quad \Delta h_{R2} = -88.73 \text{ kJ/mol} \quad \text{(R2)}$$

The enthalpies of reaction are stated in relation to 1 mol Cu_2O and assume that the reducing agents enter at 25 °C while the other reactants are at 1200 °C (Schlesinger et al., 2011). The stoichiometry shows that reducing 1 mol Cu_2O requires 1 mol H₂ instead of $\frac{1}{4}$ mol CH_4. Since 1 mol H₂ has an energy content of 241.8 kJ (LHV)

Table 1
Annual energy demands of a conventional copper plant (Aurubis, 2019).

Energy form	Unit	Annual demand
Natural gas[a]	GWh	481
Metallurgical coke[a]	GWh	48
Electricity (direct use)	GWh	552
Electricity (oxygen production)	GWh	127
Other energy sources	GWh	16
Annual production of copper	kt	473
Specific energy demand	MWh/t	2.6

[a] Energy amount stated as lower heating value (LHV).

compared to 200.6 kJ for $\frac{1}{4}$ mol CH_4, more energy is consumed when using H_2. Thus, switching from CH_4 to H_2 increases the energy demand for reduction by 20.5%. The efficiency is calculated relative to conventional operation using methane by

$$\eta_{AF,rad,H2} = \frac{\frac{1}{4}LHV_{CH4}}{LHV_{H2}} = 0.830, \tag{1}$$

where $\eta_{AF,rad,H2}$ is the efficiency for using H_2 to meet the reducing agent demand in the anode furnace instead of CH_4, LHV_{CH4} and LHV_{H2} are the lower heating values of CH_4 and H_2, respectively. The efficiency $\eta_{AF,rad,CH4}$ for using CH_4 as a reducing agent is per definition equal to 1. The hydrogen-based reduction (Reaction (R2)), however, is 58% more exothermic than the methane-based reduction (Reaction (R1)). The additional reaction enthalpy thus reduces the process heat demand (phd). Setting the additional enthalpy of reaction in relation to the LHV of the H_2 input gives the correction factor $\nu_{AF,\Delta phd,H2}$ for the process heat demand as

$$\nu_{AF,\Delta phd,H2} = \frac{\Delta h_{R1} - \Delta h_{R2}}{LHV_{H2}} = 0.135. \tag{2}$$

An overview of the efficiencies and correction factors is given in Table 2.

According to Reaction (R1), 1 mol CO_2 is released per 1 mol CH_4. Therefore, we calculate the direct CO_2 emissions of the methane-based operation with respect to the energy demand as

$$\varepsilon_{AF,CH4}^{dir} = \frac{M_{CO2}}{LHV_{CH4}} = 197.4 \left[\frac{g_{CO2}}{kWh_{CH4}}\right], \tag{3}$$

where $\varepsilon_{AF,CH4}^{dir}$ are the CO_2 emissions per kWh input of the anode furnace AF when using CH_4, M_{CO2} is the molar mass of CO_2, and LHV_{CH4} is the molar lower heating value of CH_4 (see Table 3 for the emission factors).

2.2.2. H_2 as reducing agent in slag-cleaning furnace

In the slag-cleaning furnace, slag is kept at the operating temperature by electric resistance heating while suspended matte droplets finish settling (Schlesinger et al., 2011). To maintain a low-viscosity slag, magnetite (Fe_3O_4) is reduced to FeO with coke as reducing agent because magnetite forms a solid in slag (Schlesinger et al., 2011).

As reducing agents, pulverized coal, diesel, and natural gas have been used (Sallee and Ushakov, 1999; Li et al., 2017). Bio-diesel from

Table 2
Efficiencies and correction factors of different fuels to supply the demands normalized to conventional operation: reducing agent anode furnace demand (rad), process heat demand (phd), reducing agent slag-cleaning furnace demand (rsd), process heat slag-cleaning furnace demand (phsd), and process electricity demand (eld). The energy inputs are natural gas (CH4), hydrogen (H2), coke (C), and electricity (el).

| Process	Parameter	Value
Anode Furnace (AF)	$\eta_{AF,rad,CH4}$	1
	$\eta_{AF,rad,H2}$	0.830
	$\nu_{AF,\Delta phd,H2}$	0.135
Slag-cleaning furnace (SCF)	$\eta_{SCF,rsd,C}$	1
	$\eta_{SCF,rsd,H2}$	0.814
	$\nu_{SCF,\Delta phsd,H2}$	0.114
	$\eta_{SCF,phsd,el}$	1
Process heat supply (PHS)	$\eta_{PHS,phd,CH4}$	1
	$\eta_{PHS,phd,H2}$	1
Process electricity supply (PES)	$\eta_{PES,eld,el}$	1

Table 3
Direct emission factors of the processes when using fossil fuels.

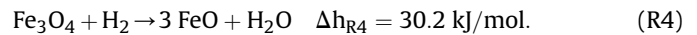| Process	Factor	Unit	Value
Anode furnace reduction (AF)	$\varepsilon_{AF,CH4}^{dir}$	g CO_2/kWh$_{CH4}$	197.4
Slag-cleaning furnace reduction (SCF)	$\varepsilon_{SCF,C}^{dir}$	g CO_2/kWh$_c$	402.6
Process heat supply (PHS)	$\varepsilon_{PHS,CH4}^{dir}$	g CO_2/kWh$_{CH4}$	197.4

waste cooking oil has also been tested as reducing agent in an industrial slag-cleaning furnace (Li et al., 2018). The corresponding analysis showed that the bio-diesel is primarily pyrolyzed to C and H_2, which then react with Fe_3O_4 in the slag. Just recently, Qu et al. (2020) have conducted experiments to analyze the reduction with H_2 by injecting a gas stream of 70% H_2 and 30% N_2 into the slag. Their results show good reduction of Fe_3O_4 and settling conditions.

Based on these applications and experiments, we assume that the switch from coke (C) to H_2 is feasible. Our calculations further assume that coke consists entirely of carbon and that utilization of both C and H_2 is 100%. Note that utilization is again likely not complete in industrial practice and will differ between reducing agents due to the differing transport phenomena, e.g., C particles gasify and create a gas film around themselves (Warczok and Riveros, 2007).

To estimate the theoretical potential of H_2 in slag reduction, the reaction

$$Fe_3O_4 + \frac{1}{2}C \rightarrow 3\,FeO + \frac{1}{2}CO_2 \quad \Delta h_{R3} = 57.8\,kJ/mol \tag{R3}$$
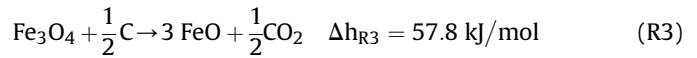
is replaced by the reaction

$$Fe_3O_4 + H_2 \rightarrow 3\,FeO + H_2O \quad \Delta h_{R4} = 30.2\,kJ/mol. \tag{R4}$$

The enthalpies of reaction are stated in relation to 1 mol Fe_3O_4 and assume that the reducing agents enter at 25 °C while the other reactants are at 1230 °C (Schlesinger et al., 2011). The stoichiometries in Reactions (R3) and (R4) show that 1 mol H_2 is necessary instead of $\frac{1}{2}$ mol C to reduce the same amount of Fe_3O_4, assuming complete reaction. The energy content of $\frac{1}{2}$ mol C and 1 mol H_2 are 196.8 kJ and 241.8 kJ, respectively. Therefore, switching the reducing agent from C to H_2 increases the energy demand by 22.9% in terms of lower heating value. The corresponding efficiencies in relation to conventional operation using C are calculated as

$$\eta_{SCF,rsd,H2} = \frac{\frac{1}{2}LHV_C}{LHV_{H2}} = 0.814, \tag{4}$$

where $\eta_{SCF,rsd,H2}$ is the efficiency for using H_2 as a reducing agent, LHV_C and LHV_{H2} are the lower heating values of C and H_2, respectively. The efficiency $\eta_{SCF,rsd,C}$ for using C as a reducing agent is per definition equal to 1. However, hydrogen-based slag reduction (Reaction (R4)) is less endothermic than coke-based reduction (Reaction (R3)) and thus requires 48% less heat. Therefore, the electrical energy input to heat the slag can be reduced accordingly. The process heat savings in relation to the H_2 input are given by the correction factor $\nu_{SCF,\Delta phsd,H2}$ as

$$\nu_{SCF,\Delta phsd,H2} = \frac{\Delta h_{R3} - \Delta h_{R4}}{LHV_{H2}} = 0.114. \tag{5}$$

The efficiency for the resistive-electric heating is assumed to be 100%, with the corresponding efficiency $\eta_{SCF,phd,el}$ being equal to 1 (Table 2).

According to Reaction (R3), 1 mol CO_2 is released per mol C. Therefore, we calculate the direct CO_2 emissions of the coke-based

operation with respect to the energy demand as

$$\varepsilon_{SCF,C}^{dir} = \frac{M_{CO2}}{LHV_C} = 402.6 \left[\frac{g_{CO2}}{kWh_C}\right], \tag{6}$$

where $\varepsilon_{SCF,C}^{dir}$ are the CO_2 emissions per kWh of the slag reduction when using carbon C, M_{CO2} is the molar mass of CO_2, and LHV_C is the heating value of C (see Table 3 for a summary of the emission factors). In contrast, Reaction (R4) with H_2 causes no direct CO_2 emissions. The indirect greenhouse gas emissions from upstream electricity supply are introduced in Section 2.4 along with other indirect upstream emissions.

2.2.3. H_2 as substitute for CH_4 in process heat supply

We assume that hydrogen burners can be used to provide process heat (Degel et al., 2019). Further, we assume that the efficiency of heat supply is 100% for both CH_4 and H_2 with regard to their lower-heating values. The respective direct CO_2 emissions for methane-based heat supply are calculated as

$$\varepsilon_{PHS,CH4}^{dir} = \frac{M_{CO2}}{LHV_{CH4}} = 197.4 \left[\frac{g_{CO2}}{kWh_{CH4}}\right], \tag{7}$$

assuming complete combustion. In Eqn. (7), $\varepsilon_{PHS,CH4}^{dir}$ are the CO_2 emissions of natural gas use (CH_4) to fulfill the process heat supply (PHS), M_{CO2} is the molar mass of CO_2, and LHV_{CH4} is the lower heating value of CH_4.

2.2.4. Utilization of electrolysis by-product O_2

One advantage of retrofitting a Power-to-H_2 system into copper production is the utilization of the electrolysis by-product O_2. Typically, the by-product O_2 is emitted to the atmosphere. When producing 1 kg of H_2 from water electrolysis, around 8 kg of O_2 are produced based on the stoichiometric reaction of water electrolysis:

$$H_2O \rightarrow H_2 + \frac{1}{2}O_2 \tag{R5}$$

Today, O_2 required for copper production is usually obtained from external production in a dedicated cryogenic air separation unit (ASU). In the investigated copper process, the annual electricity demand for the required O_2 is reported as 127 GWh (Aurubis, 2019). With a typical ASU efficiency of 200−300 kWh_{el}/t_{O2} (Banaszkiewicz et al., 2014), this energy demand corresponds to an annual O_2 demand of around 423−635 kt_{O2} of the copper production. Replacing the annual fuel demand (Table 1) with H_2 based on LHV requires around 16 kt of H_2, corresponding to around 128 kt of O_2. Even if the lower estimate for the O_2 demand is taken as reference, the electrolysis by-product O_2 can only fulfill around 30% of the O_2 demand in copper production. Thus, all by-product O_2 can be utilized and we assume that every ton of O_2 produced by the water electrolyzer substitutes a ton of O_2 otherwise produced externally, following the approach taken for O_2 utilization in other Power-to-Gas studies (Parra et al., 2017; Guilera et al., 2018; Breyer et al., 2015; Bailera et al., 2015; Kuparinen and Vakkilainen, 2017; Morgenthaler et al., 2020; Rosenfeld et al., 2020).

2.3. Power-to-H_2 system

To evaluate the techno-economic potential of a retrofit, we analyze the Power-to-H_2 system components in the following. The discussed parameters are summarized in Table 4.

Besides the Power-to-H_2 system itself, retrofitting an existing copper production plant would incur additional costs, e.g., for replacing burners or furnace equipment. However, reliably defining such cost data is difficult as the data depends on site-specific factors and non-disclosed data (Cusano et al., 2017). Therefore, we exclude costs that arise from the substitution of process equipment and point out that such costs must be added when applying the results to an existing plant.

2.3.1. Water electrolysis system

The central component of a Power-to-H_2 system is the water electrolyzer with the three main technology options: alkaline electrolysis (AEL), polymer electrolyte membrane electrolysis (PEMEL), and solid oxide electrolysis (SOEL). Generally, AEL is

Table 4
Parameters for the Power-to-H_2 system.

Component	Parameter	Unit	Value	Reference
Electrolyzer CAPEX	cpx_{EL}^{var}	EUR/kW_{el}	1000	assumption in range of [1]
Electrolyzer stack reinvest	cpx_{stk}^{var}	EUR/kW_{el}	271	45% of investment cost [2] discounted by 10 years
Electrolyzer fix. OPEX	opx_{EL}^{fix}	%-Invest/a	3	[1]
Electrolyzer lifetime system	n	a	20	assumption in range of [1]
Electrolyzer lifetime stack	n_{stk}	a	10	assumption in range of [1]
Discount rate	int	%	5.2	based on WACC from [3]
Electrolyzer efficiency	$\eta_{EL,H2,el}$	−	0.6	[1][2]
	$\eta_{EL,O2e,H2}$	kg_{O2}/kWh_{H2}	0.238	based on stoichiometric reaction, see Section 2.3
Electrolyzer min. part-load	$o_{min,EL}$	−	0.2	[1]
H_2 storage CAPEX	cpx_{H2st}^{var}	EUR/kg_{H2}	470	[4]
H_2 storage fix. OPEX	opx_{H2st}^{fix}	%-Invest/a	2.0	[4]
H_2 compressor CAPEX	cpx_{H2C}^{fix}	EUR	500,000	fit to model in [4]
	cpx_{H2C}^{var}	EUR/(kg_{H2}/h)	2440	fit to model in [4]
H_2 compressor fix. OPEX	opx_{H2C}^{fix}	%-Invest/a	1.5	[5]
H_2 compressor efficiency	$\eta_{H2C,pH2,el}$	kWh_{el}/kWh_{H2}	0.051	based on [4]
	$\eta_{H2C,pH2,H2}$	−	1	
Pressure reduction	$\eta_{VL,H2,pH2}$	−	1	assuming no H_2 losses

[1]: (Buttler and Spliethoff, 2018)   [2]: (Smolinka et al., 2018)
[3]: (KPMG, 2019)   [4]: (Chardonnet et al., 2017)
[5]: (Parra et al., 2019)

considered the most mature technology and has been available in large system sizes for a long time. PEMEL is often considered for Power-to-Gas plants, as rapid load changes are possible, allowing intermittent operation and provision of ancillary grid services (Kopp et al., 2017). SOEL is currently the least mature technology only available at high costs and small system sizes. However, SOEL technology offers very high efficiencies with a high potential for heat integration (Buttler et al., 2015).

We base the parameters of our water electrolysis system on an AEL system because AEL is the most mature technology and currently has the lowest investment cost (Buttler and Spliethoff, 2018; Parra et al., 2019; Proost, 2019). Current investment costs for AEL systems are stated in the range of 600-1500 EUR/kW$_{el}$ (Buttler and Spliethoff, 2018; Smolinka et al., 2018). We choose intermediate investment cost, also called capital expenditures (cpx), of the electrolyzer system (EL) cpx_{EL}^{var} of 1000 EUR/kW$_{el}$. It must be noted that significant scaling effects are expected when considering large water electrolysis systems (Böhm et al., 2020; IRENA, 2020). Such investment cost reductions in line with expected future developments and scaling effects will be evaluated in a detailed sensitivity analysis (cf. Section 4.3.2).

Equally important is the lifetime of the system. We differentiate between the lifetime of the electrolyzer stack and the other components. For the stack, we assume a lifetime n_{stk} of 10 years which is an average value for AEL stacks (Buttler and Spliethoff, 2018). For the other components of the Power-to-H$_2$ system, we assume a lifetime n of 20 years (Smolinka et al., 2018). Since the lifetime of the electrolyzer stack is shorter than the lifetime of the system, we include reinvestment cost for a new stack after 10 years. The cost-share of the stack is assumed to be 45% of the electrolyzer system cost (Smolinka et al., 2018). The future reinvestment cost is discounted by 10 years with an interest rate int of 5.2%, the weighted average cost of capital (WACC) for energy projects in 2018/19 (KPMG, 2019). The discounted reinvestment cost for the stack cpx_{stk}^{var} is 271 EUR/kW$_{el}$.

The operating costs include fixed and variable operating costs. Fixed operating costs, including maintenance, are often defined as an annual share of the initial investment costs. We assume fixed operational expenditures (opx) of 3%/a in our model (Buttler and Spliethoff, 2018). In contrast, the variable operating costs depend on the energy consumption and thereby on electrolyzer system efficiency. We choose a typical value for AEL systems with a system efficiency $\eta_{EL,H2,el}$ of 60 %-LHV excluding the H$_2$ compressor (Buttler and Spliethoff, 2018; Smolinka et al., 2018). The production rate of the by-product O$_2$ is calculated from the stoichiometric reaction (R5) as

$$\dot{m}_{O2,EL}\left[\frac{kg_{O2}}{h}\right] = 0.5\frac{\dot{E}_{H2,EL}}{LHV_{H2}} M_{O2} = 0.238\left[\frac{kg_{O2}}{kWh_{H2}}\right]\dot{E}_{H2,EL}, \quad (8)$$

where $\dot{m}_{O2,EL}$ is the produced material flow of O$_2$ by the electrolyzer (EL), $\dot{E}_{H2,EL}$ is the hydrogen output in terms of lower heating value, LHV$_{H2}$ is the molar energy content of hydrogen, and M$_{O2}$ is the molar mass of O$_2$. We assume that the products are supplied at an operating pressure of 30 bar, a typical value for commercially available systems (Smolinka et al., 2018; Buttler and Spliethoff, 2018).

A drawback discussed for AEL systems is the limited part-load operation. To account for that limitation in our model, we choose a typical minimal part-load $o_{min,EL}$ of 20% (Buttler and Spliethoff, 2018; Smolinka et al., 2018). It should be noted that for applications requiring fast response times and frequent system standby, e.g., ancillary grid services, another limitation of AEL systems must be considered, namely the start-up times in the order of 1–5 min

for a warm-start and 1−2 h for a cold-start (Buttler and Spliethoff, 2018). In contrast, load changes at nominal operating temperature are in the order of seconds (Buttler and Spliethoff, 2018). Since long shut-downs do not occur in our system due to the continuously operating copper production, we do not consider start-up times in the present study.

2.3.2. Pressurized H$_2$ storage

To gain more flexibility in operating the water electrolyzer, a H$_2$ storage tank is added to our model. We consider a steel storage tank to store pressurized H$_2$ at 200 bar, as such tanks are widely used in industry (Chardonnet et al., 2017). The investment costs cpx_{H2st}^{var} are assumed to be 470 EUR/kg$_{H2}$ with fixed operating costs of 2%, the current parameters for stationary storage systems (Chardonnet et al., 2017).

2.3.3. H$_2$ compressor for pressurized storage

To store H$_2$ at 200 bar, a compressor is required to increase the pressure from the 30 bar operating pressure of the electrolyzer. Due to the wide range of H$_2$ compressor configurations, investment costs vary widely in literature (van Leeuwen and Mulder, 2018). We use a variable cost function for H$_2$ compressors which depends on the compressor capacity $\dot{m}_{H2}$, compression ratio, and output pressure (Chardonnet et al., 2017). To keep the compressor cost function in our model linear, we fit a linear cost function to the model of Chardonnet et al. (2017) in the range from 0 to 40 MW$_{H2}$ throughput and a compression ratio of H$_2$ from 30 to 200 bar. The resulting investment cost for the compressor can be calculated as

$$cpx_{H2C}^{tot} = 500,000 \text{ EUR} + 2440\frac{\text{EUR}\cdot\text{h}}{kg_{H2}}\dot{m}_{H2}, \quad (9)$$

where cpx_{H2C}^{tot} is the capital expenditure of the compressor system in EUR and $\dot{m}_{H2}$ is the maximum mass flow of H$_2$ in kg/h. The corresponding fixed operating costs opx_{H2C}^{fix} are estimated as 1.5% of the initial investment costs (Parra et al., 2019).

For the operation of the compressor, we assume an electricity demand of 1.7 kWh$_{el}$/kg$_{H2}$ based on a two-stage compression from 30 to 200 bar (Chardonnet et al., 2017), which is 0.051 kWh$_{el}$/kWh$_{H2}$ based on the LHV of H$_2$ input (see $\eta_{H2C,pH2,el}$ in Table 4). We assume that there are no H$_2$ losses during compression and decompression (see $\eta_{H2C,pH2,H2}$ and $\eta_{VL,H2,pH2}$ in Table 4).

2.4. Indirect GHG emissions

Fossil fuels, electricity, and system components are associated with indirect GHG emissions from upstream processes, e.g., extraction, transport, and production, typically summarized in CO$_2$ equivalents.

For the indirect GHG emissions, we consider only the upstream emissions of commodities since the impact of the Power-to-H$_2$ components is typically small compared to the impact of electricity supply (Koj et al., 2017; Zhang et al., 2017; Bareiß et al., 2019). The total GHG emissions then consist of the direct CO$_2$ emissions of the copper production and the indirect GHG emissions. The assumptions for the upstream GHG emissions of electricity supply and commodities are presented in Table 5.

Since the electricity supply is upstream of our copper production, we refer to them as indirect GHG emissions. However, the GHG emissions of electricity supply itself are typically separated into direct and indirect emissions. For the direct GHG emissions of electricity supply, we use the emission factor $\varepsilon_{el}^{ind,dir}$ of 401 g CO$_2$-eq/kWh$_{el}$ for grid electricity in Germany in 2019 (Icha and Kuhs, 2020). For the indirect GHG emissions, we add a factor $\varepsilon_{el}^{ind,ind}$ of

Table 5
Upstream GHG emission factors of the commodities.

Commodity	Factor	Unit	Value	Reference
Electricity mix direct[a]	$\varepsilon_{el}^{ind,dir}$	g CO_2-eq/kWh$_{el}$	401.0	Icha and Kuhs (2020)
Electricity mix indirect	$\varepsilon_{el}^{ind,ind}$	g CO_2-eq/kWh$_{el}$	30.0	Wietschel et al. (2019)
Natural gas	ε_{CH4}^{ind}	g CO_2-eq/kWh$_{CH4}$	46.1	Moro and Lonza (2018)
Metallurgical coke[b]	ε_{C}^{ind}	g CO_2-eq/kWh$_c$	98.9	own calculation[b]
Oxygen from ASU[c]	ε_{O2}^{ind}	g CO_2-eq/kg$_{O2}$	80.2	own calculation[c]

[a] Average direct emission factor of grid electricity in Germany in 2019.
[b] Based on upstream coke plant emissions (Pardo et al., 2012) and LHV of coke (Suopajärvi et al., 2018).
[c] ASU efficiency of 200 kWh$_{el}$/t$_{O2}$ (Banaszkiewicz et al., 2014) and emission factor of electricity mix.

Table 6
Commodity prices.

Commodity	Parameter	Unit	Value	Reference
Electricity[a]	$p_{el,t}$	EUR/MWh	34.2	Bundesnetzagentur SMARD.de (2020)
Natural gas	$p_{CH4,t}$	EUR/MWh	28.6	Bundesnetzagentur and Bundeskartellamt (2019)
Coke	$p_{C,t}$	EUR/MWh	35.2	(Steelonthenet, 2019; Suopajärvi et al., 2018)
Oxygen	$p_{O2,t}$	EUR/t$_{O2}$	72	Pardo and Moya (2013)

[a] The shown electricity price is the average price of the historic price time series used (year 2019, German day-ahead market).

30 g CO_2-eq/kWh$_{el}$ for electricity in Germany (Wietschel et al., 2019).

2.5. Commodity prices and time of energy use

The consumption of commodities generates operating costs. In this section, we define the commodity prices and the demand profile of our reference copper production.

2.5.1. Commodity prices

The commodity prices used in our model are based on typical prices for industrial consumers in Germany in 2019 (cf. Table 6).

We assume a natural gas price of 28.6 EUR/MWh (Bundesnetzagentur and Bundeskartellamt, 2019) and a coke price of 293 EUR/t, based on the average European coke price in 2019 (Steelonthenet, 2019). Assuming an average heating value of 30 MJ/kg (Suopajärvi et al., 2018), the price for coke (C) amounts to 35.2 EUR/MWh.

To analyze the cost savings from using the electrolysis by-product O_2, we define a price for substituted O_2. We assume an oxygen price $p_{O2,t}$ of 72 EUR/t for 2020, based on a study of iron and steel production in Europe and an estimated annual growth rate of 1%/a compared to the reference year 2010 (Pardo and Moya, 2013).

Table 7
Parameters for the energy and material demands: process heat (phd), reducing agent anode furnace (rad), reducing agent slag-cleaning furnace (rsd), process heat slag-cleaning furnace (phsd), process electricity demand (eld), and oxygen (O2d). The parameters are calculated based on the annual demands from Aurubis (2019) and operating parameters from Schlesinger et al. (2011), as explained in Section 2.5.

Demand	Parameter	Unit	Value	Profile
Process heat	$\dot{D}_{phd,t}$	MW	47.7	Constant
Reducing agent AF	$\dot{D}_{rad,t}$	MW	12.0	Intermittent[a]
Reducing agent SCF	$\dot{D}_{rsd,t}$	MW	5.5	Constant
Electricity for process heat SCF	$\dot{D}_{phsd,t}$	MW	3.0	Constant
Other electricity demand	$\dot{D}_{eld,t}$	MW	60.0	Constant
Oxygen	$\dot{D}_{O2d,t}$	t/h	72.6	Constant

[a] The intermittent demand profile is shown in Fig. 2.

This value fits into price ranges for O_2 in Power-to-Gas studies ranging from 50 EUR/t$_{O2}$ (Kuparinen and Vakkilainen, 2017; Rosenfeld et al., 2020) to 150 EUR/t$_{O2}$ (Guilera et al., 2018), with several studies also lying in the middle of this range (Parra et al., 2017; Breyer et al., 2015; Pardo and Moya, 2013; Graf et al., 2014).

For the electricity prices, we use the 2019 historic day-ahead spot market prices in Germany with hourly resolution (Bundesnetzagentur — SMARD.de, 2020). The average electricity price $p_{el,t}$ was 34.2 EUR/MWh. We use wholesale electricity prices because Power-to-Gas systems in combination with energy-intensive industry are largely exempted from electricity tax and levies in Germany (Chardonnet et al., 2017). Following Felgenhauer and Hamacher (2015), we assume that the cost of water is negligible.

2.5.2. Energy and material demands

In this section, we present the assumed energy and material demands of our reference copper production plant throughout the year (Table 7).

The time to process one batch of 270 t of copper in an anode furnace is 9 h (Schlesinger et al., 2011). The reduction with natural gas is one sub-task which lasts 3 h while consuming 120 m³/h (Schlesinger et al., 2011). Since we consider an annual production of 473,040 t copper (cf. Table 1) (Aurubis, 2019), the overall production consists of around 1,752 batches. These batches are refined by two anode furnaces (Schlesinger et al., 2011). We assume that the two anode furnaces operate in an alternating manner (cf. Fig. 2). The alternating operation causes an intermittent natural gas demand of $\dot{D}_{rad,t}$ of 12.0 MW during the reduction.

The slag-cleaning furnace continuously treats slag coming from the smelter (Schlesinger et al., 2011). Thus, we assume that the slag-cleaning furnace has a steady-state demand for coke. Based on the annual coke demand (Table 1), the hourly coke demand $\dot{D}_{rsd,t}$ is 5.5 MWh. Additionally, the slag-cleaning furnace has a power demand of 3 MW to heat the slag.

Due to a lack of public data, we assume a constant aggregated process heat demand, which is calculated from the annual natural gas demand (cf. Table 1) minus the gas used as reducing agent. The resulting annual process heat demand is 417.9 GWh, which
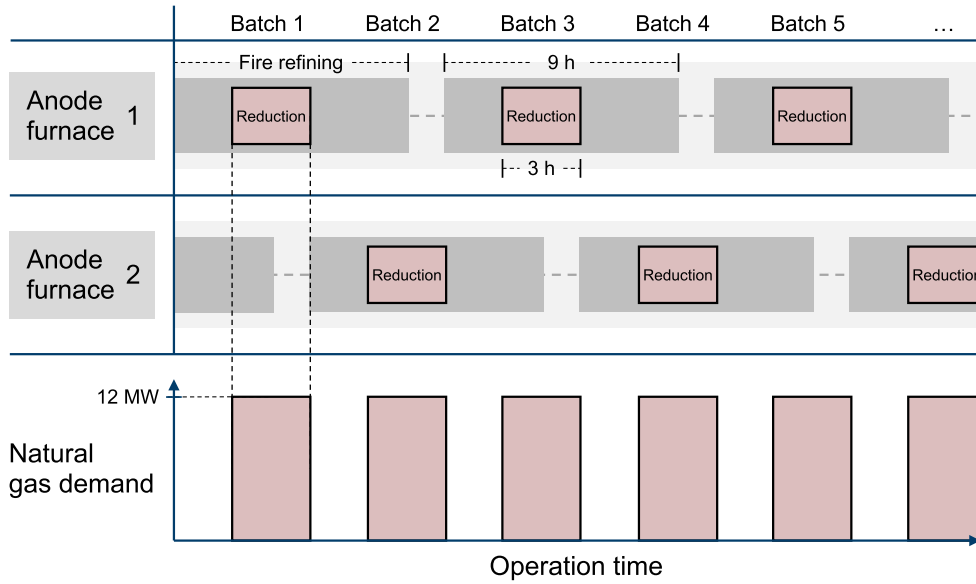
Fig. 2. Intermittent natural gas demand profile as reducing agent in the anode furnace.

corresponds to a steady-state demand of process heat $\dot{D}_{\text{phd,t}}$ of 47.7 MW.

Oxygen is primarily used for the oxygen enrichment of the blast in the flash furnace. Since the flash furnace runs continuously and due to the lack of detailed operating data, we assume a steady-state oxygen demand. We calculate the O_2 demand from the electricity consumption of a modern air separation unit (Table 1) with an efficiency of 200 kWh/t of O_2 (Banaszkiewicz et al., 2014). The corresponding O_2 demand $\dot{D}_{\text{O2d,t}}$ is 72.6 t/h.

The annual electricity demand of our reference copper production plant (Table 1) corresponds to an average steady-state demand of 63 MW. Since we analyze the slag-cleaning furnace separately, we have to subtract the 3 MW electricity demand for heating the slag. Thus, all other electricity consumers correspond to an electricity demand $\dot{D}_{\text{eld,t}}$ of 60 MW.

3. Method and problem description

To evaluate the benefits of retrofitting a Power-to-H_2 into copper production, we use mathematical optimization.

3.1. Optimization formulation

We use mixed-integer linear programming (MILP) to optimize the design and operation of the Power-to-H_2 system. MILP is an optimization method that minimizes a given linear objective function subject to a set of linear constraints (Nemhauser and Wolsey, 1988). The optimization variables include both discrete decisions, e.g., whether to install a certain component, and continuous decisions, e.g., the size of a component or the level of operation at a certain point of time. Design problems where both investment and the operating costs shall be optimized can often be stated as (piece-wise) linear models and solved efficiently to global optimality by MILP (Grossmann, 1985; Voll et al., 2013).

3.1.1. Objective: total annualized cost (TAC)

The objective of our optimization is to minimize the total annualized cost (TAC) of the retrofit. The TAC includes investment and operating costs over a project lifetime of 20 years. The objective is written as

$$min \sum_{c \in \mathscr{C}} \left(CPX_c \cdot CRF + OPX_c^{\text{fix}} \right) + \sum_{t \in \mathscr{T}} \sum_{s \in \mathscr{S}} OPX_{s,t}^{\text{var}} \cdot \Delta t, \quad (10)$$

where CPX_c is the capital expenditure for the investment cost of component c with $\mathscr{C}$ as the set of all components, CRF is the capital recovery factor which converts initial investment cost to annual cost based on project lifetime n and discount rate int. Based on n and int, we calculate the capital recovery factor as

$$CRF = \frac{(1 + int)^n \cdot int}{(1 + int)^n - 1}. \quad (11)$$

In the objective (10), OPX_c^{fix} are the fixed operating expenditures, i.e., maintenance cost. $OPX_{s,t}^{\text{var}}$ are the variable cost which arise from consuming commodity s in time step t. Set $\mathscr{S}$ contains all commodity sources and set $\mathscr{T}$ contains the 8760 hourly time steps of the year. The operating costs are multiplied by Δt which is the uniform duration of each time step and set to 1 h.

The capital expenditure CPX or investment cost for a component is calculated as

$$CPX_c = y_c \, cpx_c^{\text{fix}} + P_c^{\text{N}} \, cpx_c^{\text{var}} \quad \forall \, c \in \mathscr{C}, \quad (12)$$

where the binary variable y_c takes the value 1 if a component is installed, cpx_c^{fix} is the fixed investment cost, P_c^{N} is the component size, and cpx_c^{var} is the size-specific investment cost.

The annual fixed operating expenditure OPX_c^{fix} of a component c is determined by

$$OPX_c^{\text{fix}} = CPX_c \cdot opx_c^{\text{fix}} \quad \forall \, c \in \mathscr{C}, \quad (13)$$

where CPX_c is the initial investment cost of component c, and opx_c^{fix} is a factor for the annual operation and maintenance cost independent of operation.

In contrast, the variable operating expenditure $OPX_{s,t}^{\text{var}}$ depends on the actual operation. $OPX_{s,t}^{\text{var}}$ arises when commodities are consumed and is calculated as

$$OPX_{s,t}^{\text{var}} = p_{s,t}\, \dot{S}_{s,t} \quad \forall\, s\in\mathscr{S},\ t\in\mathscr{T}, \tag{14}$$

where $p_{s,t}$ is the price of commodity s in time step t, $\dot{S}_{s,t}$ is the amount of commodity consumed.

3.1.2. Constraints

The copper production process has to be supplied by the necessary energy and materials of reducing agents, oxygen, process heat, and electricity (cf. Table 1). To this end, we formulate a system-wide balance equation for each type of energy and material in each time step as

$$\sum_{c\,\in\,C} \dot{E}_{e,c,t} + \dot{S}_{s,t} = \dot{D}_{d,t} \quad \forall\, e\in\mathscr{S}\cup\mathscr{I}\cup\mathscr{D},\ s\in\mathscr{S},\ d\in\mathscr{D},\ t\in\mathscr{T}, \tag{15}$$

where $\dot{E}_{e,c,t}$ describes the energy/material flow e to/from component c in time step t, $\dot{S}_{s,t}$ are the flows from source s supplying the system with a commodity, $\dot{D}_{d,t}$ represents the energy or material demand d.

The demand set $\mathscr{D}$ contains demands that have to be fulfilled in every time step t to not hinder copper production. The six considered demands are: process heat, oxygen, reducing agent for the anode furnace, reducing agent for the slag-cleaning furnace, electricity for process heat in the slag-cleaning furnace, and other electricity demands. The set $\mathscr{S}$ contains four sources available in the model: electricity, natural gas, metallurgical coke, and oxygen.

Components transform materials and energy from the sources to fulfill the demands of the system. The installation of components is described as

$$y_c\, P_c^{\min} \le P_c^{N} \le y_c\, P_c^{\max} \quad \forall\, c\in\mathscr{C}, \tag{16}$$

where y_c is the binary decision to install component c with $P_c^{\min}$ and $P_c^{\max}$ as the minimal and maximal installation size. $P_c^{\min}$ is set to 0 MW and $P_c^{\max}$ is chosen sufficiently high with 1000 MW to not influence the optimal solution.

To determine the operation rate $P_{c,t}^{O}$ of a component in each time step, we formulate operating constraints as

$$x_{c,t}\, P_c^{N}\, o_c^{\min} \le P_{c,t}^{O} \le x_{c,t}\, P_c^{N} \quad \forall\, c\in\mathscr{C},\ t\in\mathscr{T}, \tag{17}$$

where $x_{c,t}$ is the binary decision to operate the component in time step t, and $o_c^{\min}$ is the minimal part-load factor of component c. As Eqn. (17) contains a bi-linear product of a binary variable and a continuous variable, i.e., $x_{c,t}$ and P_c^{N}, we reformulate the bi-linear term based on Glover (1975).

The operation of a component is connected to the energy and material flows by

$$\dot{E}_{e_o,c,t} = P_{c,t}^{O}, \quad \forall\, c\in\mathscr{C},\ t\in\mathscr{T}, \tag{18}$$

$$\dot{E}_{e_o,c,t} = \eta_{c,e_o,e_i}\, \dot{E}_{e_i,c,t} \quad \forall\, c\in\mathscr{C},\ t\in\mathscr{T}, \tag{19}$$

where $\dot{E}_{e_o,c,t}$ is the main material/energy output and η_{c,e_o,e_i} denotes the efficiency of transforming e_i into e_o. Note that a component may have multiple in- and outputs, e.g., the water electrolyzer has one input (electricity) and two outputs (H_2 and O_2).

Based on the input of H_2 as reducing agent, the correction factors $\nu_{c,\Delta e_o,H2}$ determine the reduction in process heat demand as

$$\dot{E}_{\Delta\text{phd,AF},t} = \nu_{\text{AF},\Delta\text{phd,H2}}\, \dot{E}_{\text{H2,AF},t} \quad \forall\, t\in\mathscr{T}, \tag{20}$$

$$\dot{E}_{\Delta\text{phsd,SCF},t} = \nu_{\text{SCF},\Delta\text{phsd,H2}}\, \dot{E}_{\text{H2,SCF},t} \quad \forall\, t\in\mathscr{T}, \tag{21}$$

where $\dot{E}_{\Delta\text{phd,AF},t}$ and $\dot{E}_{\Delta\text{phsd,SCF},t}$ are the amounts of process heat reduction, and $\dot{E}_{\text{H2,AF},t}$ and $\dot{E}_{\text{H2,SCF},t}$ are the corresponding inputs of H_2 as reducing agent based on LHV.

To enable a flexible operation of the water electrolyzer, a H_2 storage tank (H2st) is part of the Power-to-H_2 system. The state of charge (SOC) of the H_2 storage is obtained from

$$SOC_{t+1} = SOC_t + \dot{E}_{\text{pH2,H2st},t}\cdot\Delta t \quad \forall\, t\in\mathscr{T}\setminus\{8760\}, \tag{22}$$

$$1 = x_{\text{storage-in,t}} + x_{\text{storage-out,t}} \quad \forall\, t\in\mathscr{T}, \tag{23}$$

$$SOC_{8760} = SOC_0, \tag{24}$$

where SOC_{t+1} is the state of charge based on the state of charge SOC_t from the previous time step and the in- or output $\dot{E}_{\text{pH2,H2st},t}$ of pressurized H_2 in time step t. The storage can only charge or discharge at a time (Eqn. (23)). The initial state of charge is a variable and Equation (24) enforces that the final state of charge (end of year) is equal to the initial state of charge (beginning of year).

3.1.3. GHG emissions

Direct CO_2 emissions are emitted when fossil fuel is consumed by a component. The arising CO_2 output contributes to the direct CO_2 emissions of the overall system. The hourly system-wide direct CO_2 emissions $CO_{2_t}^{\text{dir}}$ are calculated by summing over the different components and sources, i.e.,

$$CO_{2_t}^{\text{dir}} = \sum_{s\,\in\,\mathscr{S}}\sum_{c\,\in\,\mathscr{C}} \varepsilon_{s,c}^{\text{dir}}\, \dot{E}_{s,c,t} \quad \forall\, t\in\mathscr{T}, \tag{25}$$

and the annual direct CO_2 emissions CO_2^{dir} are calculated as

$$CO_2^{\text{dir}} = \sum_{t\,\in\,\mathscr{T}} CO_{2_t}^{\text{dir}} \tag{26}$$

$$CO_2^{\text{dir}} \le CO_2^{\text{AL}}, \tag{27}$$

where $\dot{E}_{s,c,t}$ is the material consumption of component c in time step t, $\varepsilon_{c,s}$ is the emission factor when component c consumes s, e.g., natural gas. The parameter CO_2^{AL} in Eqn. (27) limits the annual direct CO_2 emissions CO_2^{dir}. We vary the limit CO_2^{AL} to analyze different degrees of decarbonization. The optimizer chooses how and when to reduce CO_2 to determine the most cost-efficient design and operation for a given annual limit CO_2^{AL}.

The indirect GHG emissions are calculated as

$$GHG^{\text{ind}} = \sum_{t\,\in\,\mathscr{T}}\sum_{s\,\in\,\mathscr{S}} \varepsilon_s^{\text{ind}}\, \dot{S}_{s,t}, \tag{28}$$

where $\varepsilon_s^{\text{ind}}$ is the indirect emission factor corresponding to the commodity consumption $\dot{S}_{s,t}$ in time step t.

Finally, the total GHG emissions are computed by

$$GHG^{\text{tot}} = CO_2^{\text{dir}} + GHG^{\text{ind}}. \tag{29}$$

3.2. Successive decarbonization

Our reference scenario is defined as conventional production and energy supply based on fossil fuels as well as electricity from the grid. We then investigate different degrees of decarbonization by imposing limits on the allowed direct CO_2 emissions (CO_2^{AL}) corresponding to emission reductions from 5% to 100% in increments of 5% (see Fig. 3). The CO_2 limit is defined as

$$CO_2^{AL} = \alpha \cdot CO_2^{conv}, \tag{30}$$

where α is the share of CO_2 emissions allowed in relation to the emissions from conventional operation CO_2^{conv} which correspond to an α of 1 (100%). The CO_2 limitation makes the retrofit with the Power-to-H_2 system necessary as it allows to replace coke and/or natural gas by H_2 (Section 2.2). To chart a successive design path for decarbonization, the results of the previous optimization are used as lower bound of the design decisions y_c and P_c^{min} (Eqn. (16)) in the successive optimization with tighter CO_2 limit. Thereby, the designs build on each other.

As a key figure of each scenario, we define the direct CO_2 abatement cost (AC) as

$$AC = \frac{\Delta TAC}{\Delta CO_2^{dir}}, \tag{31}$$

where ΔTAC is the increase of total annualized cost (TAC) of the retrofitted production in comparison to the reference case, and ΔCO_2^{dir} is the annual reduction of direct CO_2 emissions compared to the reference case. Analogously, we calculate the total GHG abatement cost based on the total GHG emissions.

4. Results and discussion

In this section, we evaluate the potential of Power-to-H_2 to decarbonize copper production for various degrees of decarbonization. First, we analyze the economic potential and system design in Section 4.1. Second, we assess the environmental impact with regard to GHG emissions in Section 4.2. Last, in Section 4.3, the sensitivity of the results towards several techno-economic parameters is evaluated and set into relation to expected future technological advancements.

4.1. Decarbonizing copper production

We analyze the optimal results for decarbonizing a copper production with a Power-to-H_2 system under today's technical parameters and prices. To rank the economic efficiency of decarbonizing the sub-tasks of our copper production, we analyze the results of optimized systems under increasingly strict CO_2 limits.

With increasing CO_2 emission reduction from 5% to 100%, the resulting direct CO_2 abatement cost for the retrofit increases from 112 to 201 EUR/t CO_2, see Fig. 4(a).

These abatement costs vastly exceed current European Union Allowances (EUA) that had an average price of 24.6 EUR/t CO_2 in 2019 on the European Energy Exchange (EEX, 2019). However, CO_2 prices are expected to increase in the future as governments take more action on climate change. While the expected future CO_2 prices vary strongly between different scenarios and models (Rogelj et al., 2018), a European scenario projects up to 310 EUR/t CO_2 in 2050 (EU Commission, 2011). Such a price is consistent with studies considering the 1.5 °C climate change mitigation goals (Rogelj et al., 2018).

Meanwhile, costs for CO_2 higher than the current EUA prices are already in place in some countries today, e.g., in Sweden with 110 EUR/t CO_2 (Government Offices of Sweden, 2020) or in Switzerland with 90 EUR/t CO_2 in 2018 (Bundesamt für Umwelt, 2019).

Breakdowns of the direct CO_2 abatement costs are shown in Fig. 4(a). As expected, the electricity cost for the Power-to-H_2 system is the largest cost factor of the retrofit with 70% for the complete elimination of direct CO_2 emissions. Therefore, we analyze the impact of different electricity prices in a sensitivity analysis. Further, we find that the utilization of the O_2 by-product has a substantial positive economic impact on the direct CO_2 abatement cost, reducing costs by 81 EUR/t CO_2 in the 100% reduction case. Thus, the utilization of the water electrolysis by-product O_2 reduces the direct CO_2 abatement cost by 29% compared to a system that emits the O_2. The results make a strong case for retrofitting Power-to-H_2 on-site at a plant with large O_2 demand. Furthermore, it can be seen that the investment cost of the H_2 storage system is negligible. The electricity cost of the compressor is small as well, compared to the water electrolyzer with only 0.15% of the electricity cost of the supplied H_2.
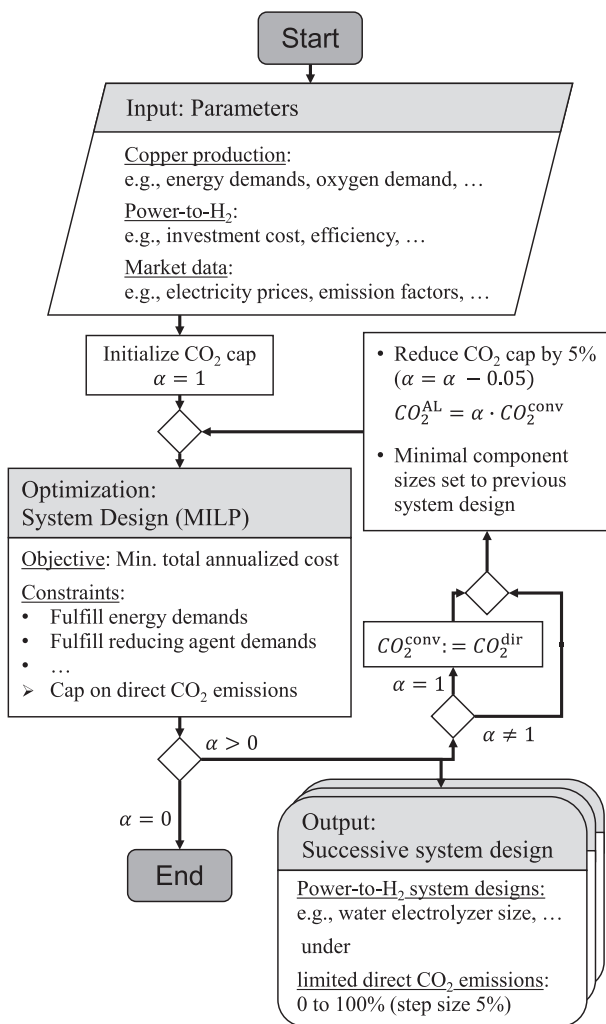

Fig. 3. Solution procedure of the successive decarbonization of copper production. The rhomboid represents input data. Rectangles without a heading describe actions. The rectangle with heading represents the design optimization. The rhombi mark branches in the procedure with the corresponding condition written at the outgoing arrow. The rectangles with rounded corners represent the collected results: the optimal system designs.
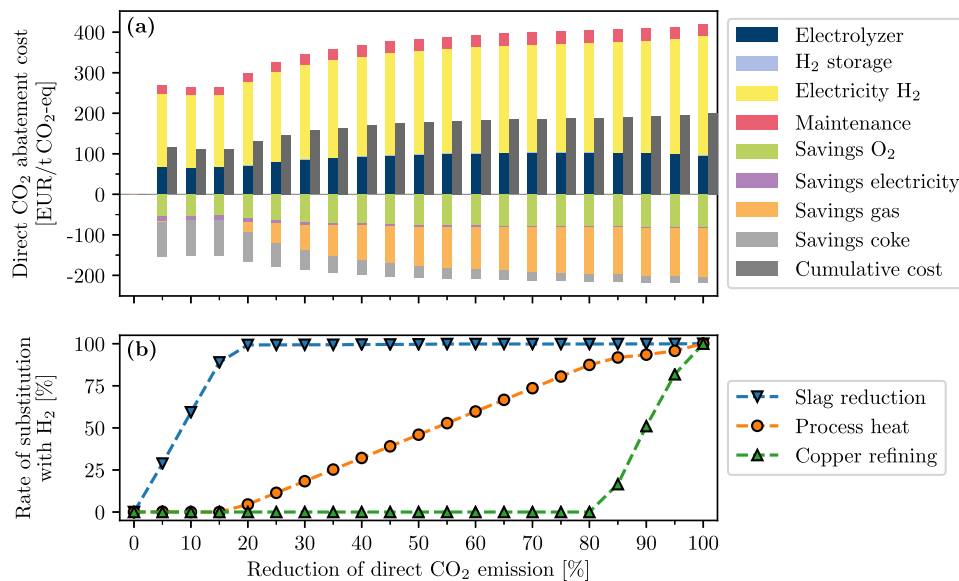
Fig. 4. Results of the decarbonization of copper production by retrofitting a Power-to-H_2 system. (a) The resulting direct CO_2 abatement cost for increasingly tighter direct CO_2 emission limits ranging from the conventional process (0% reduction) to the fully-decarbonized process (100% reduction). (b) The degree of substitution with H_2. The substitution is defined as the share of H_2 in the total energy demand.
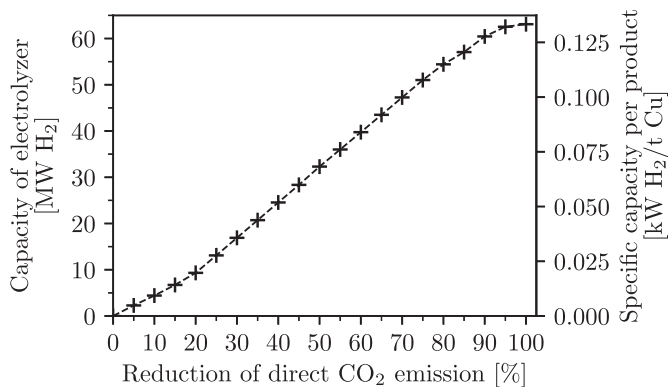

Fig. 5. Electrolyzer peak capacity in terms of hydrogen output (LHV). The left axis shows the total peak capacity and the right axis shows the peak capacity in relation to the annual copper production volume.

Table 8
Power-to-H_2 system design in the fully-decarbonized case.

Component	Unit	Value
Water electrolyzer	MW_{H2}	63.1
H_2 compressor	MW_{H2}	8.7
H_2 storage capacity	MWh_{H2}	77.8
H_2 initial filling level (t = 0)	MWh_{H2}	24.5

Fig. 6. Influence of the electricity prices (a) on the electrolyzer operation (b) and state of charge of the H_2 storage over the first week of the year (c). The solid ellipse (c) marks the effect of the intermittent demand of the anode furnace reducing agent. The dashed ellipses mark an example of discharging the storage in hours of high electricity prices followed by slow recharging of the storage. The dashed line in the electrolyzer operation (b) marks the minimal active part-load.

Fig. 4(b) shows the degree of H_2 usage which is defined as the share of H_2 in the annual energy demand of the respective process. When imposing a CO_2 limit, the first process to switch to H_2 is the slag-reduction task because of the large direct CO_2 emissions from the reduction with coke. The use of H_2 in the slag-reduction quickly reaches 99% and only in the fully-decarbonized case reaches 100%. The 99% threshold occurs because the water electrolyzer is shut down during the highest electricity price peaks in the year and coke is used instead.

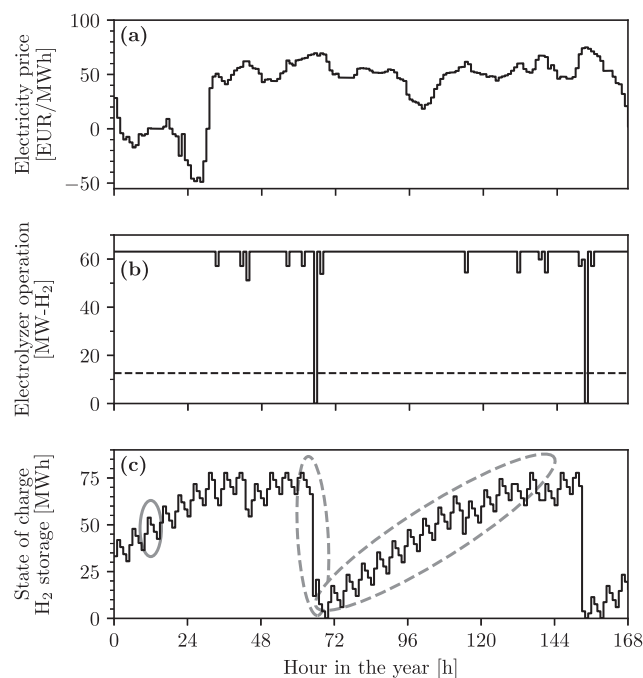When almost all coke is substituted, H_2 is also used to supply

process heat (Fig. 4(b)). The stagnation of the H_2 use for process heat at around 85−90% reduction is caused by a change in system design: When the copper refining in the anode furnace starts to use H_2, a larger H_2 storage is introduced to balance the uneven demand profile of the copper refining (Fig. 2). Therefore, it becomes cheaper

to use H_2 for copper refining than for increasing H_2 usage in process heat supply during times of high electricity prices.

Fig. 5 shows the optimal electrolyzer capacity for varying degree of decarbonization. To enable comparisons with other electrolysis applications, we set the electrolyzer capacity in relation to the annual copper production volume (Fig. 5, right axis).

The resulting design for the Power-to-H_2 system in the fully-decarbonized case shows that the optimal storage is small compared to the electrolyzer output with a capacity corresponding to 1.23 h of operation, see Table 8. This design decision is attributed to the relatively constant energy demand of the process, the additional costs for the storage system, and most importantly, the necessary over-sizing of the electrolyzer for intermittent production of stock H_2 for later use.

Fig. 6 shows the state of charge (SOC) for the H_2 storage during the first week in the year. The storage is slowly charged during times of low electricity prices and discharged within few hours of high electricity prices (e.g. hours 64 to 68). The pattern of rapid discharging followed by slow charging repeats itself throughout the year. The electrolyzer operation (Fig. 6(b)) shows the economic advantage of adding H_2 storage: the system can react to variable electricity prices. Beyond this pattern, the state of charge also reveals a shorter charging and discharging pattern which is caused by the intermittent demand for reducing agent in the copper refining (Fig. 6(c)). In our model, a potential energy demand of the electrolyzer during system standby is neglected, as we observe that standby occurs only in 69 h of the year and never lasts longer than 1 h. The additional annual electricity demand for hot-standby mode would amount to just $0.008-0.04\%$ of the annual electrolyzer electricity demand, assuming typical values for standby energy demand of $1-5\%$ of nominal load (Smolinka et al., 2018). We want to note, however, that in systems with more frequent or extensive standby operation, electrolyzer technology allowing for fast startup times and thus complete shutdowns avoiding standby losses might be advantageous.

An analysis of the H_2 cost structure (Fig. 7) shows that initial investment and electricity costs dominate. The resulting cost for the H_2 is around 2.65 EUR/kg$_{H2}$ which is similar to the study by Chardonnet et al. (2017), which finds H_2 costs of 2.4 EUR/kg for a large-scale water electrolysis system supplying an oil refinery. Note that the system in Chardonnet et al. (2017) considers an oversized water electrolyzer which enables even lower electricity prices. However, the main reason for the relatively low H_2 price are the low electricity prices both in our investigation and their study. The electricity prices are based on direct procurement on the wholesale day-ahead market and tax exemption (Section 2.5.1).

Besides the cost of hydrogen, the additional cost related to the final product copper are most relevant for the economic operation of a plant. Fig. 8 shows the increase in copper production cost due
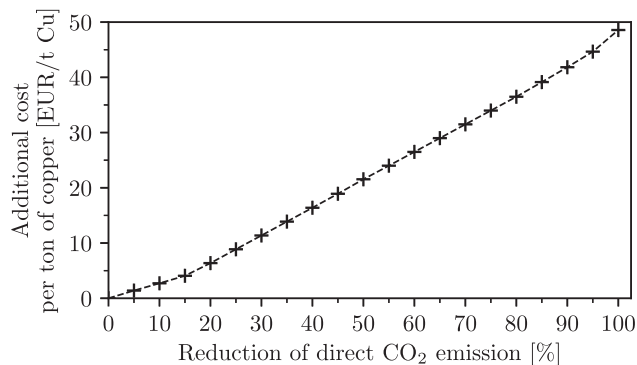
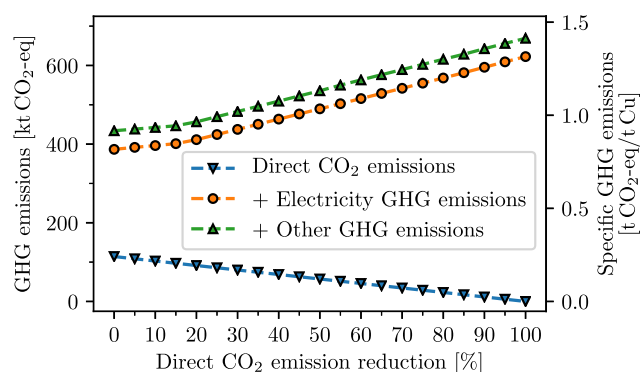**Fig. 8.** The additional total annualized cost per ton of copper.

Fig. 9. Direct CO_2 plus indirect GHG emissions of copper production with Power-to-H_2 retrofit. The GHG emissions of electricity include only the direct emissions of grid electricity in Germany in 2019 (Icha and Kuhs, 2020). The other GHG emissions further include upstream emissions from electricity supply and other commodities, i.e., natural gas and coke. The left axis shows the annual GHG emissions and the right axis shows the annual GHG emissions in relation to the annual copper production volume.

to decarbonization by Power-to-H_2. While the cost per ton of copper may appear small compared to typical copper market prices, the actual revenue realized for smelting and refining (around 435 EUR/t Cu in February 2020 (Aurubis, 2020)) is significantly smaller than the copper market price. This revenue is calculated from treatment and refining charges as well as premiums for the sale of copper cathodes (Aurubis, 2020), as these make up the main revenue of a smelter (Díaz-Borrego et al., 2019). Therefore, the shown additional cost corresponds to up to 11% of the main revenue when the production is fully decarbonized, thus constituting a relevant cost factor.

4.2. Total GHG emissions

Fig. 9 shows the impact of direct CO_2 emission reductions on the GHG emissions of our copper production retrofitted by Power-to-H_2.

A major part of the total GHG emissions originates from upstream processes even in the conventional system (74%), most notably from electricity generation. For grid electricity, we differentiate between direct emissions from electricity supply with 401 g CO_2-eq/kWh$_{el}$ (Icha and Kuhs, 2020) and indirect emissions from processes upstream of electricity supply with 30 g CO_2-eq/kWh$_{el}$ (Wietschel et al., 2019). The remaining indirect GHG emissions in our analysis are from the upstream processes for natural gas and
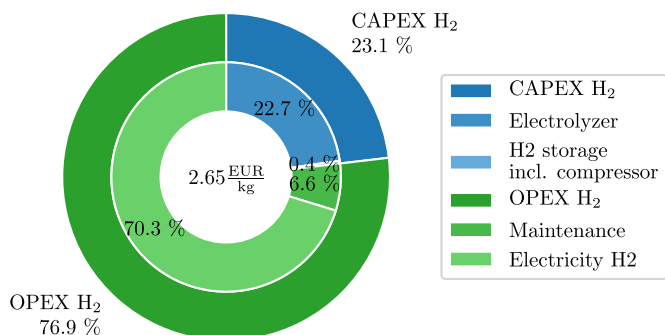
Fig. 7. Cost structure of the produced H_2 in the fully-decarbonized scenario.
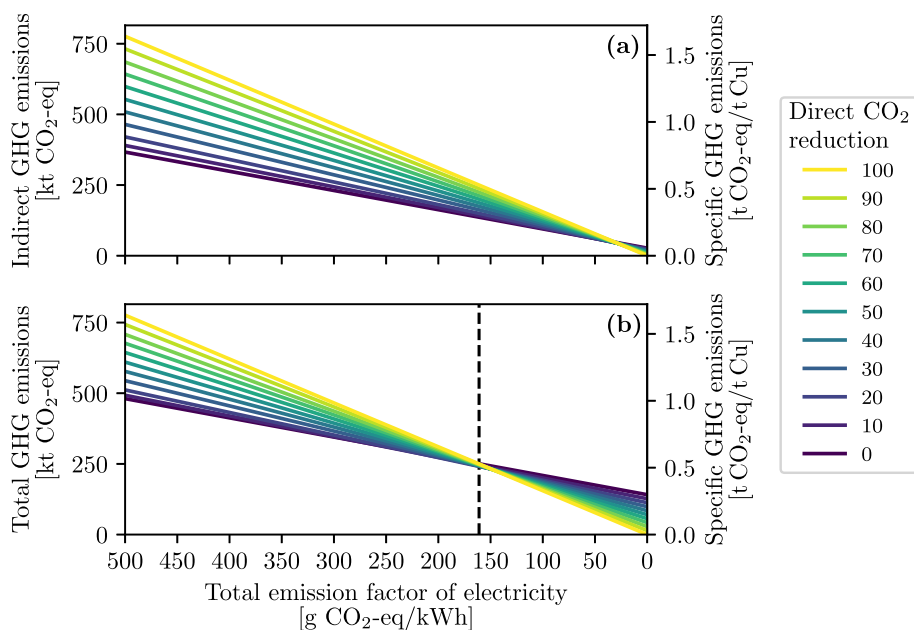
Fig. 10. Impact of the emission factor of electricity on the indirect (a) and total GHG emissions (b). The dashed line shows the point of intersection between the conventional production and the fully-decarbonized production. The left axes show the annual GHG emissions and the right axes show the annual GHG emissions in relation to the annual copper production volume.

coke supply. The specific emissions of the conventional operation (0.92 t CO_2-eq/t Cu) in our model agree well with the reported direct and indirect CO_2 emissions (0.96 t CO_2-eq/t Cu) of the reference plant (Aurubis, 2019). These climate impacts are small compared to the average climate change impacts reported for copper production (Dong et al., 2020), since only the production plant is considered and not the mining operations for copper ore concentrate which make up a large part of the overall climate change impact, especially at low ore grades (Norgate and Haque, 2010). For a production process using the same technologies as our model, Reuter et al. (2015) and Abadías Llamas et al. (2019) determined the climate change impact of the complete production chain, including the mining operations with copper ore grades

of 1% and 0.7% Cu, to account for 2.6 and 2.7 t CO_2-eq/t Cu, respectively. These climate impacts are in the lower range of values of copper production reported by Dong et al. (2020). While the analyzed plant thus already represents a modern and very efficient plant in Europe, it remains important to further reduce emissions in view of the growing global copper demand.

For the Power-to-H_2 system, GHG emissions from electricity supply exceed the avoided emissions from natural gas and coke of a decarbonized system (Fig. 9). Thus, running the Power-to-H_2 system using today's German electricity mix would increase total GHG emissions.

In view of the evolving decarbonization of the electricity supply, we analyze the impact of lower electricity emission factors in increments of 50 g CO_2-eq/kWh$_{el}$ (Fig. 10).

A decreasing total emission factor for grid electricity also reduces the total GHG emissions of the conventional copper production due to the high electricity demand of the conventional process. The scenario with 150 g CO_2-eq/kWh$_{el}$ is the first instance where total GHG emissions of the fully-decarbonized copper production are lower than for conventional copper production. A linear interpolation shows that the crossover point between the conventional and the fully-decarbonized copper production lies at 160 g CO_2-eq/kWh$_{el}$. Thus, only if the GHG emissions from the electricity supply are below 160 g CO_2-eq/kWh$_{el}$, decarbonization of copper production with Power-to-H_2 has not only a local but also a positive global impact on GHG emissions.

Since the total GHG emissions strongly depend on the upstream emissions of electricity supply, we further evaluate the abatement cost in relation to avoided total GHG emissions (Fig. 11). The copper plant is assumed to have reduced all direct emissions. Because total GHG emissions are reduced only if the emission factor of electricity is below 160 g CO_2-eq/kWh$_{el}$ (Fig. 10), we focus our total GHG abatement cost analysis on values below this threshold. As expected, the total GHG abatement cost strongly depends on the total emission factor of electricity. Further, we see that the total GHG abatement cost is much higher than the direct CO_2 abatement cost and only reaches similar cost at low-emission electricity with
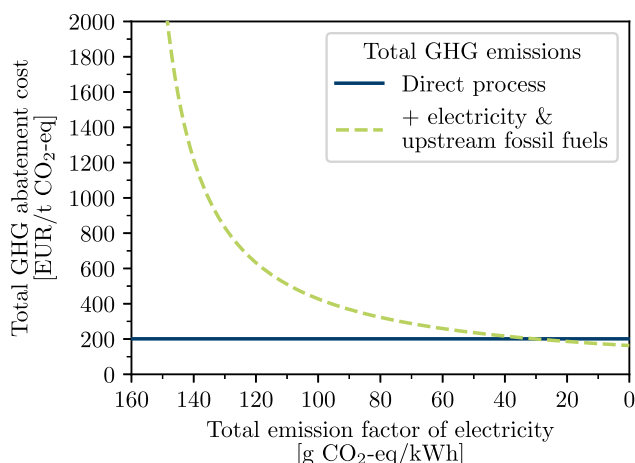

Fig. 11. Total GHG abatement cost for complete decarbonization of copper production by Power-to-H_2, i.e., 100% reduction of direct emissions. The remaining indirect GHG emissions of electricity are based on the total emission factor of electricity and the fossil fuels consider the avoided upstream GHG emissions from natural gas and coke supply.
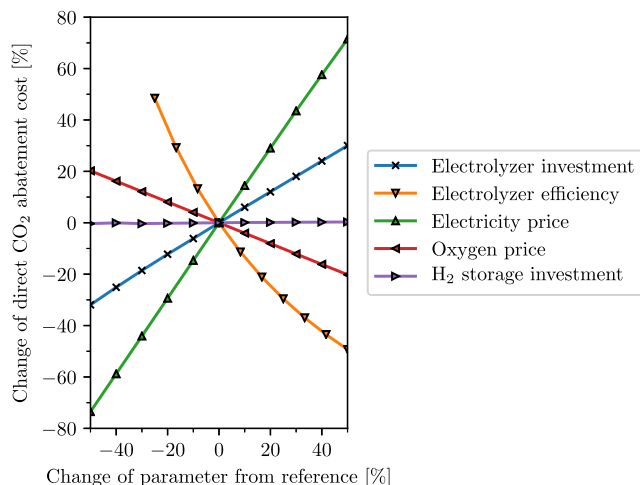
Fig. 12. Sensitivity analysis for the fully-decarbonized system. The values are set in relation to the reference case with direct CO_2 abatement cost of 201 EUR/t CO_2.

Fig. 13. Total direct CO_2 abatement cost under varied parameters: (a) electrolyzer investment cost and (b) electrolyzer efficiency.

around 30 g CO_2-eq/kWh$_{el}$. Beyond that value, the total GHG abatement cost can drop below the direct CO_2 emission abatement cost due to the avoided emissions from upstream natural gas and coke supply, which are not considered in the direct CO_2 emissions.

4.3. Future technology developments

Some parameters in our model are likely to change in the future due to technological progress. Most importantly, water electrolysis systems are expected to be further improved leading to lower investment cost (Thema et al., 2019; Buttler and Spliethoff, 2018; Smolinka et al., 2018) and higher efficiency, e.g., by commercialization of large SOEL systems (Buttler and Spliethoff, 2018). Commodity prices, most notably for grid electricity and O_2, are also subject to change and influence the economic feasibility of the Power-to-H_2 retrofit. We, therefore, conduct a sensitivity analysis on the influence of prices for O_2 and electricity, water electrolyzer efficiency and investment cost, as well as H_2 storage investment cost on the direct CO_2 abatement cost.

4.3.1. Sensitivity analysis

Fig. 12 shows that the direct CO_2 abatement cost is very sensitive to changes in the electricity cost. This result is not surprising as electricity costs dominate the cost structure (Fig. 7). Any change in electricity prices through power generation, procurement strategies, taxes or tax exemptions can have a huge influence on the profitability of decarbonization by Power-to-H_2. Thus, the economics of decarbonization depend strongly on the local electricity market conditions. An electricity price increase of 10%, for instance, results in additional abatement cost of 29 EUR/t CO_2 (14.5%).

The second most influential parameter is the efficiency of the electrolyzer system, which influences both investment cost and operating cost by reducing the necessary electrolyzer size as well as the electricity demand. Thus, any potential improvement in the efficiency has a large influence on the direct CO_2 abatement cost. Assuming an electrolyzer system can improve its efficiency by 5% in absolute terms, e.g., from 60 to 65% system efficiency (corresponding to a relative increase of 8%), the abatement cost decrease by 23 EUR/t CO_2 (11.3%).

The investment cost of the electrolyzer system has the third strongest influence on the direct CO_2 abatement cost. A decrease of 100 EUR/kW$_{el}$ (10%) reduces the direct CO_2 abatement cost by 12
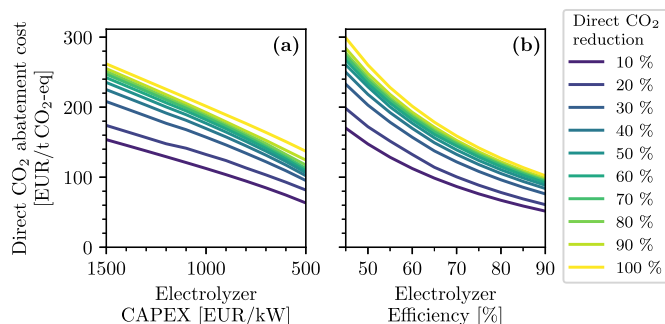
EUR/t CO_2 (6.1%).

Increasing the O_2 price by 10% decreases the abatement cost by 8 EUR/t CO_2 (4.1%) due to the higher economic benefit from the avoided O_2 procurement cost.

The shown investment cost of the hydrogen storage system includes both costs for H_2 storage and compressor. However, the influence of the H_2 storage on the direct CO_2 abatement cost is negligible. An increase of the storage system cost of 10% increases the direct CO_2 abatement cost by only 0.2 EUR/t CO_2 (0.1%). Interestingly, the H_2 storage is designed larger in scenarios with low electrolyzer investment cost as over-sizing becomes more attractive. When the electrolyzer investment cost is reduced by 10%, the optimal storage size increases by about 53%.

4.3.2. Impact of water electrolysis development

Since technical and economic performance of water electrolysis systems are expected to improve in the future, we analyze the impact of such developments on the direct CO_2 abatement cost by Power-to-H_2.

To analyze the impact of decreasing water electrolyzer investment cost, we analyze the direct CO_2 abatement cost over a typical range of investment costs (Fig. 13(a)). The investment costs range from 1500 to 500 EUR/kW$_{el}$, which represents the range from an expensive alkaline-electrolyzer system today down to future AEL and PEMEL systems (Smolinka et al., 2018). Assuming investment cost of 500 EUR/kW$_{el}$ for the electrolyzer system, the direct CO_2 abatement cost reaches 136 EUR/t CO_2 to avoid all direct emissions.

The slight non-linearity in the direct CO_2 abatement cost curve is a result of the electrolyzer becoming larger in scenarios with lower investment cost. The larger size allows for more operational freedom to exploit fluctuating electricity prices and thus can save operating cost.

The efficiency of electrolyzer systems is also expected to improve in the future and has a large impact on the direct CO_2 abatement cost (cf. Fig. 13(b)). The costs decrease to 127 EUR/t CO_2 for an electrolyzer system efficiency of 80%, a value corresponding to existing SOEL systems with heat integration (Buttler and Spliethoff, 2018; Sunfire GmbH, 2020), e.g., a system with saturated steam input at 150°C and 3 bar achieves an electric efficiency of 82% (LHV) (Sunfire GmbH, 2020). However, the higher investment cost of SOEL systems counteracts cost reductions in electricity costs achieved by higher efficiencies.

The non-linearity in the direct CO_2 abatement cost curve as a function of electrolyzer efficiency is caused by the efficiency influencing both investment and operating costs: a higher efficiency allows for a smaller electrolyzer and less electricity consumption during operation.

As both investment cost and efficiency of water electrolysis systems are expected to improve, we analyze a combined
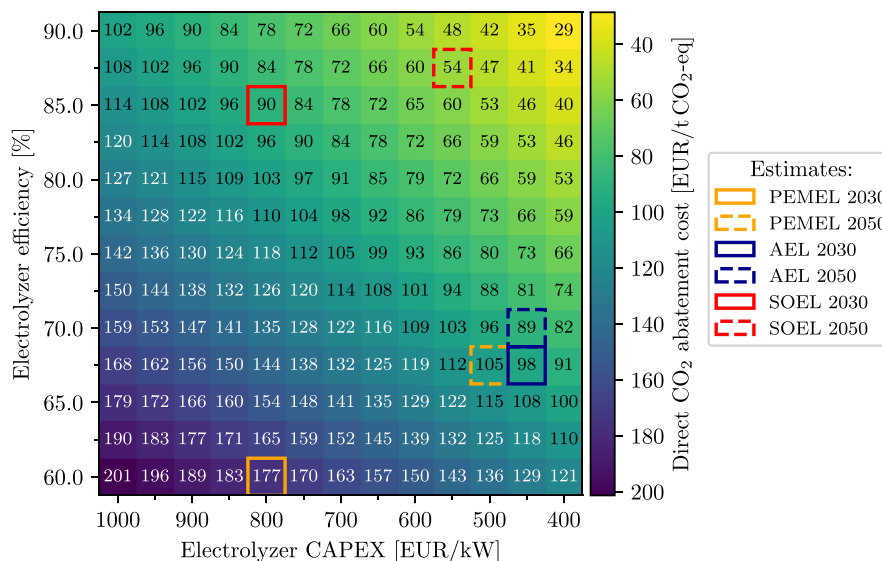
Fig. 14. Direct CO_2 abatement cost under decreasing electrolyzer investment cost and increasing efficiency. Highlighted estimates for the electrolyzer system parameters are taken from Smolinka et al. (2018). To display the estimations on our parameter grid, we rounded each value to the nearest increment in our sensitivity analysis. The stated efficiency of the solid oxide electrolysis (SOEL) does not consider the energy for steam generation (Smolinka et al., 2018).
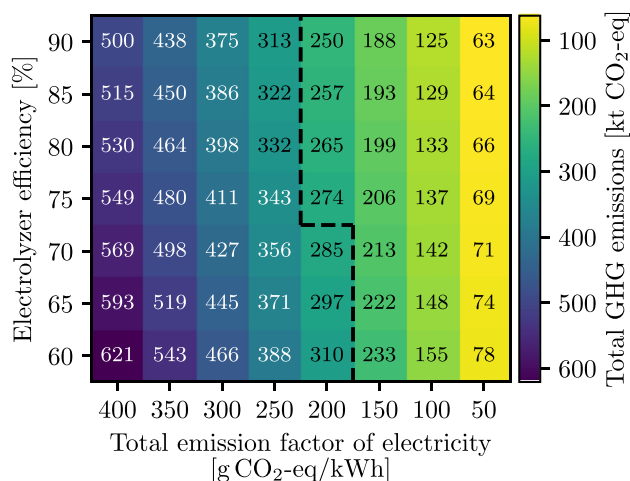

Fig. 15. Total GHG emissions under decreasing emission factor of the electricity supply and increasing electrolyzer efficiency. The dashed line marks the threshold where the total GHG emissions of the fully-decarbonized process decrease in comparison to the conventional production process.

development of both parameters. The parameter pairs and the resulting direct CO_2 abatement cost are presented in Fig. 14. We highlight typical estimates for future electrolyzer systems based on the parameterized data set given in Smolinka et al. (2018). The highlighted results show three electrolyzer technologies: alkaline (AEL), polymer electrolyte membrane (PEMEL), and solid oxide electrolysis (SOEL) in 2030 and 2050.

The potential commercialization of SOEL systems is often considered to result in high efficiencies and large cost reductions, with some estimates even below 500 EUR/kW$_{el}$ in the long-term (Bertuccioli et al., 2014; Smolinka et al., 2018). We find that the combination of both parameters can drastically reduce the direct CO_2 abatement cost to a value of 54 EUR/t CO_2 for a system expected in 2050.

AEL and PEMEL systems are also expected to improve in the short-term (2030) and long-term (2050) (Smolinka et al., 2018). The estimates for 2030 already imply strong reductions in the direct CO_2 abatement cost. The AEL reaches direct CO_2 abatement cost of around 98 EUR/t CO_2 in 2030. While the abatement cost for the PEMEL is noticeably higher in 2030, it reaches a value of 105 EUR/t CO_2 in 2050, similar to the 89 EUR/t CO_2 for the AEL in 2050.

The expected future improvement of the electrolyzer efficiency also has an impact on the total GHG emissions (Fig. 15). With increasing efficiency, the system consumes less electricity which reduces the indirect GHG emissions from the electricity supply. Since the emission factor of the electricity supply is expected to improve in the future, we also analyze its impact.

While an increase in electrolyzer efficiency has a positive impact on the total GHG emissions, it becomes clear that the emission factor of the supplied electricity is absolutely crucial. The dashed line in Fig. 15 marks the threshold at which the retrofit becomes overall positive in comparison to the conventional copper production in terms of total GHG emissions. Thus, a drastic reduction of GHG emissions in the electricity supply is of utmost importance to support the decarbonization of copper production by Power-to-H$_2$. In summary, the results emphasize that the supply with renewable electricity is by far the most important factor to reduce total GHG emissions even if considering improvements in electrolyzer efficiency.

4.4. Discussion and implications

We now discuss the significance and implications of our work from an economic and environmental perspective, as well as the importance for different stakeholders.

While our model is based on a specific process design (Section 2.1), the process setup consists of the most commonly applied technologies in copper production. Thus, we expect our main findings in combination with the given sensitivity analysis to apply to a broad range of copper plants. In addition, the disclosure of our model equations, parameters, and assumptions enables readers with access to plant-specific data to adapt our analysis to their

particular plant and site. With access to additional data not publicly available, the model could also be updated to account for potential impacts beyond those we could assess, e.g., non-ideal fuel utilization rates.

The determined potential provides industry stakeholders with a first estimate of the cost of decarbonizing copper production by hydrogen and shows the beneficial co-utilization of the electrolysis by-product O_2. The direct CO_2 abatement cost of 201 EUR/t CO_2 gives an indication under which cost of CO_2 the retrofit becomes profitable. Vice versa, the findings show policy makers the incentives or carbon prices that need to be put in place to encourage industry to decarbonize.

Our results show that the cost of decarbonization constitutes a relevant cost factor in copper production. To prevent carbon leakage by making production regionally unprofitable, border carbon adjustment might be necessary. Preserving regional copper production capacities with low GHG footprints can be especially important for the goal of a circular economy since copper production is of great importance for the recycling of electronic waste and recovery of valuable minor elements (Reuter et al., 2019).

Future improvements in water electrolysis technology would greatly reduce the economic cost of decarbonization. High-temperature electrolysis with heat integration offers particular high efficiencies. Cooperation between potential customers of large-scale electrolyzers such as copper producers and manufacturers of such systems is beneficial as the estimated cost reductions are in parts based on learning effects from installed systems (Böhm et al., 2020). The expected cost reduction together with higher CO_2 certificate prices might lead to a reinforcing effect by making Power-to-H_2 system for decarbonization of industries economically feasible.

As our analysis has once again confirmed, the electricity price is a critical factor for cost-efficient decarbonization of energy-intensive industries by Power-to-H_2. Moreover, the required electricity must come from low-carbon sources, as the overall emissions are highly dependent on the emission factors of electricity supply and in case of copper production only decrease with electricity emission factors below 160 g CO_2-eq/kWh. Therefore, assessment of the local electricity supply conditions is always required to determine the overall GHG emissions reduction potential for such a retrofit. Future works should therefore include specific local emission factors as the local situation can vary strongly from the case for Germany laid out here. Many smelters are located near the sea to receive ore shipments (Schlesinger et al., 2011) and proximity to off-shore wind parks could potentially offer opportunities to access low-carbon power.

While the on-site integration of a Power-to-H_2 system shows a great economic benefit by reducing the direct CO_2 abatement cost by 81 EUR/t CO_2, imported H_2 that is produced in optimal locations with high full-load hours for wind and solar power generation represents an interesting alternative that should be investigated in a future study. Considering H_2 production facilities in remote locations may also become necessary due to the high demand for renewable electricity when decarbonizing industry, as shown for the chemical industry (Kätelhön et al., 2019), which could readily exceed regional renewable energy potentials.

5. Conclusions

This work analyzes the techno-economic potential of decarbonizing copper production with H_2 by retrofitting a Power-to-H_2

system to eliminate direct CO_2 emissions. The total greenhouse gas (GHG) emissions are determined to evaluate the climate change impact of the retrofit.

The results show direct CO_2 abatement cost of around 201 EUR/t CO_2 assuming current Power-to-H_2 technologies and commodity costs in Germany (2019). This direct CO_2 abatement cost vastly exceeds the average price of European Union Allowances (EUA) of 24.6 EUR/t CO_2 in 2019. However, future prices of up to 310 EUR/t CO_2 in 2050 are estimated in a scenario by the European Union to mitigate climate change. Other studies find that similar prices for CO_2 emissions are necessary for climate change mitigation in the future, indicating that the Power-to-H_2 route might become viable in the future.

While the profitability depends strongly on the price of electricity, the savings from utilizing the electrolysis by-product O_2 in the copper plant have a substantial positive impact on the direct CO_2 abatement cost. This result makes on-site integration of Power-to-H_2 and copper production more attractive than separate operation sites. Co-utilization of H_2 and O_2 also reduces GHG emissions as less O_2 has to be supplied by cryogenic air separation. While the hydrogen storage system has little impact on the abatement cost, storage allows the water electrolyzer to react to the electricity prices to some extent. While the storage capacity is sized rather small compared to the peak power of the electrolyzer in our study, we expect the storage to have a larger economic impact in case of more severe electricity price fluctuations.

While direct CO_2 emissions can be avoided by retrofitting a Power-to-H_2 system, our results show that the retrofit reduces total GHG emissions only if the emission factor of electricity is below 160 g CO_2-eq/kWh.

The sensitivity analysis shows that expected future developments of water electrolysis systems in terms of technical and economic performance can drastically reduce the direct CO_2 abatement cost. Reduced investment cost and efficiency gains of alkaline electrolyzers expected already for 2030 halve the direct CO_2 abatement cost to around 98 EUR/t CO_2. Most promising is the commercialization of large solid oxide electrolyzer systems (SOEL) with heat integration, enabling direct CO_2 abatement cost of around 90 EUR/t CO_2 expected in 2030 and 54 EUR/t CO_2 expected in 2050.

Based on the progress of water electrolysis technology and rising future CO_2 certificate prices, it seems likely that the decarbonization of copper production by a Power-to-H_2 system retrofit will become profitable in the next decades. However, decarbonization of the electricity supply will be crucial to lower the total GHG emissions of copper production.

Further research should focus on the local conditions of the energy supply as we observe strong impacts of electricity prices and emission factors. Our model and analysis can easily be adapted to a specific plant or site by updating the relevant model parameters. The model should also be refined by learnings from experimental implementations of hydrogen in copper production. Since renewable energy is key for a successful decarbonization but intermittent in nature, copper production equipped with a Power-to-H_2 system including H_2 storage may also represent a potentially valuable source of demand-side flexibility.

CRediT authorship contribution statement

Fritz T.C. Röben: Conceptualization, Methodology, Software, Formal analysis, Validation, Visualization, Writing − original draft. **Nikolas Schöne:** Methodology, Software, Formal analysis,

Visualization, Writing − review & editing. **Uwe Bau:** Conceptualization, Supervision, Writing − review & editing. **Markus A. Reuter:** Funding acquisition, Writing − review & editing. **Manuel Dahmen:** Conceptualization, Supervision, Writing − review & editing. **André Bardow:** Funding acquisition, Conceptualization, Supervision, Writing − review & editing.

Declaration of competing interest

The authors declare that they have no known competing financial interests or personal relationships that could have appeared to influence the work reported in this paper.

Acknowledgements

References

Abadías Llamas, A., Valero Delgado, A., Valero Capilla, A., Torres Cuadra, C., Hultgren, M., Peltomaeki, M., Roine, A., Stelter, M., Reuter, M.A., 2019. Simulation-based exergy, thermo-economic and environmental footprint analysis of primary copper production. Miner. Eng. 131, 15. https://doi.org/10.1016/j.mineng.2018.11.007.

Aurubis, 2019. Environmental protection in the Aurubis group. Report. Aurubis AG. https://www.aurubis.com/binaries/content/assets/aurubis-en/dateien/responsibility/environmental-statement/2019_aurubis_ag_environmental_statement_en.pdf. Accessed: 2019-12-18.

Aurubis, 2020. Copper mail no. 181. Report. Aurubis AG. https://www.aurubis.com/en/investor-relations/news-and-reports/copper-mail/copper-mail-update. Accessed: 2021-02-16.

Bailera, M., Lisbona, P., Romeo, L.M., 2015. Power to gas-oxyfuel boiler hybrid systems. Int. J. Hydrogen Energy 40, 10168−10175. https://doi.org/10.1016/j.ijhydene.2015.06.074.

Banaszkiewicz, T., Chorowski, M., Gizicki, W., 2014. Comparative analysis of oxygen production for oxy-combustion application. Energy Procedia 51, 127−134. https://doi.org/10.1016/j.egypro.2014.07.014.

Bareiß, K., de la Rua, C., Möckl, M., Hamacher, T., 2019. Life cycle assessment of hydrogen from proton exchange membrane water electrolysis in future energy systems. Appl. Energy 237, 862−872. https://doi.org/10.1016/j.apenergy.2019.01.001.

Bertuccioli, L., Chan, A., Hart, D., Lehner, F., Madden, B., Standen, E., 2014. Study on development of water electrolysis in the EU. Report. E4tech Sàrl with Element Energy Ltd for the Fuel Cells and Hydrogen Joint Undertaking. https://www.fch.europa.eu/node/783. Accessed: 2020-02-26.

Böhm, H., Zauner, A., Rosenfeld, D.C., Tichler, R., 2020. Projecting cost development for future large-scale power-to-gas implementations by scaling effects. Appl. Energy 264, 114780. https://doi.org/10.1016/j.apenergy.2020.114780.

Bonnin, M., Azzaro-Pantel, C., Domenech, S., 2019. Optimization of natural resource management: application to French copper cycle. J. Clean. Prod. 223, 252−269. https://doi.org/10.1016/j.jclepro.2019.03.081.

Breyer, C., Tsupari, E., Tikka, V., Vainikka, P., 2015. Power-to-gas as an emerging profitable business through creating an integrated value chain. Energy Procedia 73, 182−189. https://doi.org/10.1016/j.egypro.2015.07.668.

Brunner, C., Michaelis, J., Möst, D., 2015. Competitiveness of different operational concepts for power-to-gas in future energy systems. Z. Energiewirtschaft 39, 275−293. https://doi.org/10.1007/s12398-015-0165-0.

Bundesamt für Umwelt, 2019. CO2 Abgabe. Web page. https://www.bafu.admin.ch/bafu/de/home/themen/klima/fachinformationen/klimapolitik/co2-abgabe.html. Accessed: 2020-03-19.

Bundesnetzagentur, Bundeskartellamt, 2019. Monitoringbericht 2019. Report. Bundesnetzagentur und Bundeskartellamt. https://www.bundesnetzagentur.de/SharedDocs/Mediathek/Berichte/2019/Monitoringbericht_Energie2019.pdf. Accessed: 2019-12-16.

Bundesnetzagentur | SMARD.de, 2020. SMARD Strommarktdaten. Web page. Bundesnetzagentur. https://www.smard.de/. Accessed: 2020-02-13.

Buttler, A., Koltun, R., Wolf, R., Spliethoff, H., 2015. A detailed techno-economic analysis of heat integration in high temperature electrolysis for efficient hydrogen production. Int. J. Hydrogen Energy 40, 38−50. https://doi.org/10.1016/j.ijhydene.2014.10.048.

Buttler, A., Spliethoff, H., 2018. Current status of water electrolysis for energy storage, grid balancing and sector coupling via power-to-gas and power-to-liquids: a review. Renew. Sustain. Energy Rev. 82, 2440−2454. https://doi.org/10.1016/j.rser.2017.09.003.

Chardonnet, C., Giordano, V., Rapoport, S., De Vos, L., Genoese, F., Roig, G., Bart, F., Lanoix, J.C., Vanhoudt, W., De Lacroix, T., Ha, T., Van Genabet, B., 2017. Study on early business cases for H2 in energy storage and more broadly power to H2 applications. Report. FCH 2 JU. https://www.fch.europa.eu/sites/default/files/

P2H_Full_Study_FCHJU.pdf. Accessed: 2020-04-23.

de Coninck, H., Revi, A., Babiker, M., Bertoldi, P., Buckeridge, M., Cartwright, A., Dong, W., Ford, J., Fuss, S., Hourcade, J.C., Ley, D., Mechler, R., Newman, P., Revokatova, A., Schultz, S., Steg, L., Sugiyama, T., 2018. Implementing and strengthening the global response. In: Masson-Delmotte, V., Zhai, P., Pörtner, H.O., Roberts, D., Skea, J., Shukla, P.R., Pirani, A., Moufouma-Okia, W., Péan, C., Pidcock, R., Connors, S., Matthews, J.B.R., Chen, Y., Zhou, X., Gomis, M.I., Lonnoy, E., Maycock, T., Tignor, M., Waterfield, T. (Eds.), Global Warming of 1.5°C. An IPCC Special Report on the Impacts of Global Warming of 1.5°C above Pre-industrial Levels and Related Global Greenhouse Gas Emission Pathways, in the Context of Strengthening the Global Response to the Threat of Climate Change, Sustainable Development, and Efforts to Eradicate Poverty. Intergovernmental Panel on Climate Change, pp. 313−443.

Cusano, G., Gonzalo, M.R., Farrell, F., Remus, R., Roudier, S., Sancho, L.D., 2017. Best available techniques (BAT) reference document for the non-ferrous metals industries. Report. European Comission, Industrial Emissions Directive. https://doi.org/10.2760/8224.

Deetman, S., Pauliuk, S., van Vuuren, D.P., van der Voet, E., Tukker, A., 2018. Scenarios for demand growth of metals in electricity generation technologies, cars, and electronic appliances. Environ. Sci. Technol. 52, 4950−4959. https://doi.org/10.1021/acs.est.7b05549.

Degel, R., Lux, T., Hecker, E., Filzwieser, A., Krassnig, H.J., Filzwieser, I., 2019. Innovative solutions in non-ferrous metals production. In: Proceedings of the 58th Annual Conference of Metallurgists (COM) Hosting the 10th International Copper Conference 2019, Vancouver, Canada, 18-21 August 2019. The Canadian Institute of Mining, Metallurgy and Petroleum.

Dong, D., van Oers, L., Tukker, A., van der Voet, E., 2020. Assessing the future environmental impacts of copper production in China: implications of the energy transition. J. Clean. Prod. 274, 122825 https://doi.org/10.1016/j.jclepro.2020.122825.

Díaz-Borrego, F.J., Miras-Rodríguez, M.d.M., Escobar-Pérez, B., 2019. Looking for accurate forecasting of copper TC/RC benchmark levels. Complexity 1−16. https://doi.org/10.1155/2019/8523748, 2019.

EEX, 2019. Emission spot primary market auction report 2019. Report. European Energy Exchange. https://www.eex.com/en/market-data/environmental-markets/eua-primary-auction-spot-download. Accessed: 2020-02-19.

Elshkaki, A., Graedel, T.E., Ciacci, L., Reck, B.K., 2016. Copper demand, supply, and associated energy use to 2050. Global Environ. Change 39, 305−315. https://doi.org/10.1016/j.gloenvcha.2016.06.006.

EU Commission, 2011. Energy Roadmap 2050. Impact Assessment and Scenario Analysis. Report SEC, 1565. EU.

Felgenhauer, M., Hamacher, T., 2015. State-of-the-art of commercial electrolyzers and on-site hydrogen generation for logistic vehicles in South Carolina. Int. J. Hydrogen Energy 40, 2084−2090. https://doi.org/10.1016/j.ijhydene.2014.12.043.

Fischedick, M., Marzinkowski, J., Winzer, P., Weigel, M., 2014a. Techno-economic evaluation of innovative steel production technologies. J. Clean. Prod. 84, 563−580. https://doi.org/10.1016/j.jclepro.2014.05.063.

Fischedick, M., Roy, J., Acquaye, A., Allwood, J., Ceron, J.P., Geng, Y., Kheshgi, H., Lanza, A., Perczyk, D., Price, L., Santalla, E., Sheinbaum, C., Tanaka, K., 2014b. Industry. In: Edenhofer, O., Pichs-Madruga, R., Sokona, Y., Farahani, E., Kadner, S., Seyboth, K., Adler, A., Baum, I., Brunner, S., Eickemeier, P., nad Kriemann, B., Savolainen, J., Schlömer, S., von Stechow, C., Zwickel, T., Minx, J.C. (Eds.), Climate Change 2014: Mitigation of Cimate Change. Contribution of Working Group III to the Fifth Assessment Report of the Intergovernmental Panel on Climate Change. Cambridge University Press, Cambridge, United Kingdom and New York, NY, USA, pp. 739−810.

Friedmann, S.J., Fan, Z., Tang, K., 2019. Low-carbon Heat Solutions for Heavy Industry: Sources, Options, and Costs Today. Report. Columbia SIPA Center on Global Energy Policy. URL: https://energypolicy.columbia.edu/sites/default/files/file-uploads/LowCarbonHeat-CGEP_Report_100219-2_0.pdf. (Accessed 30 October 2019).

Glover, F., 1975. Improved linear integer programming formulations of nonlinear integer problems. Manag. Sci. 22, 455−460. https://doi.org/10.1287/mnsc.22.4.455.

Government Offices of Sweden, 2020. Sweden's carbon tax. https://www.government.se/government-policy/taxes-and-tariffs/swedens-carbon-tax. Accessed: 2020-03-19.

Goyal, P., Themelis, N.J., Zanchuk, W.A., 1982. Gaseous refining of anode copper. JOM The Journal of The Minerals, Metals & Materials Society (TMS) 34, 22−28. https://doi.org/10.1007/BF03338157.

Graf, F., Krajete, A., Schmack, U., 2014. Abschlussbericht - Techno-ökonomische Studie zur biologischen Methanisierung bei Power-to-Gas-Konzepten. Report. Deutscher Verein des Gas- und Wasserfaches e.V. https://www.dvgw.de/themen/forschung-und-innovation/forschungsprojekte/dvgw-forschungsbericht-g-30113/. Accessed: 2019-04-30.

Grossmann, I.E., 1985. Mixed-integer programming approach for the synthesis of integrated process flowsheets. Comput. Chem. Eng. 9, 463−482. https://doi.org/10.1016/0098-1354(85)80023-5.

Guilera, J., Ramon Morante, J., Andreu, T., 2018. Economic viability of SNG production from power and CO2. Energy Convers. Manag. 162, 218−224. https://doi.org/10.1016/j.enconman.2018.02.037.

Henckens, M.L.C.M., Worrell, E., 2020. Reviewing the availability of copper and nickel for future generations. The balance between production growth, sustainability and recycling rates. J. Clean. Prod. 264, 121460. https://doi.org/

10.1016/j.jclepro.2020.121460.

Icha, P., Kuhs, G., 2020. Entwicklung der spezifischen Kohlendioxid-Emissionen des deutschen Strommix in den Jahren 1990 - 2019. Report Climate Change 13/2020. Umweltbundesamt. https://www.umweltbundesamt.de/en/publikationen/entwicklung-der-spezifischen-kohlendioxid-6. Accessed: 2020-07-15.

IRENA, 2020. Green Hydrogen Cost Reduction: Scaling up Electrolysers to Meet the 1.5°C Goal. Report. International Renewable Energy Agency, Abu Dhabi.

Kätelhön, A., Meys, R., Deutz, S., Suh, S., Bardow, A., 2019. Climate change mitigation potential of carbon capture and utilization in the chemical industry. Proc. Natl. Acad. Sci. Unit. States Am. 116, 11187. https://doi.org/10.1073/pnas.1821029116.

Koj, J.C., Wulf, C., Schreiber, A., Zapp, P., 2017. Site-dependent environmental impacts of industrial hydrogen production by alkaline water electrolysis. Energies 10, 860. https://doi.org/10.3390/en10070860.

Kopp, M., Coleman, D., Stiller, C., Scheffer, K., Aichinger, J., Scheppat, B., 2017. Energiepark Mainz: technical and economic analysis of the worldwide largest Power-to-Gas plant with PEM electrolysis. Int. J. Hydrogen Energy 42, 13311–13320. https://doi.org/10.1016/j.ijhydene.2016.12.145.

KPMG, 2019. Cost of capital study 2019. Report. KPMG AG. https://home.kpmg/de/en/home/insights/2019/10/cost-of-capital-study-2019.html. Accessed: 2020-03-02.

Kuipers, K.J.J., van Oers, L.F.C.M., Verboon, M., van der Voet, E., 2018. Assessing environmental implications associated with global copper demand and supply scenarios from 2010 to 2050. Global Environ. Change 49, 106–115. https://doi.org/10.1016/j.gloenvcha.2018.02.008.

Kulczycka, J., Lelek, Ł., Lewandowska, A., Wirth, H., Bergesen, J.D., 2016. Environmental impacts of energy-efficient pyrometallurgical copper smelting technologies: the consequences of technological changes from 2010 to 2050. J. Ind. Ecol. 20, 304–316. https://doi.org/10.1111/jiec.12369.

Kuparinen, K., Vakkilainen, E., 2017. Green pulp mill: renewable alternatives to fossil fuels in lime kiln operations. BioResources 12, 4031–4048. https://doi.org/10.15376/biores.12.2.4031-4048.

van Leeuwen, C., Mulder, M., 2018. Power-to-gas in electricity markets dominated by renewables. Appl. Energy 232, 258–272. https://doi.org/10.1016/j.apenergy.2018.09.217.

Li, B., Wang, X., Wang, H., Wei, Y., Hu, J., 2017. Smelting reduction and kinetics analysis of magnetic iron in copper slag using waste cooking oil. Sci. Rep. 7, 2406. https://doi.org/10.1038/s41598-017-02696-y.

Li, B., Wei, Y., Wang, H., Yang, Y., 2018. Reduction of magnetite from copper smelting slag using petro-diesel and biodiesel. ISIJ Int. 58, 1168–1174. https://doi.org/10.2355/isijinternational.ISIJINT-2017-723.

Luderer, G., Vrontisi, Z., Bertram, C., Edelenbosch, O.Y., Pietzcker, R.C., Rogelj, J., De Boer, H.S., Drouet, L., Emmerling, J., Fricko, O., Fujimori, S., Havlík, P., Iyer, G., Keramidas, K., Kitous, A., Pehl, M., Krey, V., Riahi, K., Saveyn, B., Tavoni, M., Van Vuuren, D.P., Kriegler, E., 2018. Residual fossil CO2 emissions in 1.5–2°C pathways. Nat. Clim. Change 8, 626–633. https://doi.org/10.1038/s41558-018-0198-6.

Marin, T., Utigard, T., 2010. Deoxidation of liquid copper with reducing O2/CH4 flames. Metall. Mater. Trans. B 41, 535–542. https://doi.org/10.1007/s11663-010-9346-8.

Moreno-Leiva, S., Haas, J., Junne, T., Valencia, F., Godin, H., Kracht, W., Nowak, W., Eltrop, L., 2019. Renewable energy in copper production: a review on systems design and methodological approaches. J. Clean. Prod. 246, 118978. https://doi.org/10.1016/j.jclepro.2019.118978.

Morgenthaler, S., Ball, C., Koj, J.C., Kuckshinrichs, W., Witthaut, D., 2020. Site-dependent levelized cost assessment for fully renewable power-to-methane systems. Energy Convers. Manag. 223, 113150. https://doi.org/10.1016/j.enconman.2020.113150.

Moro, A., Lonza, L., 2018. Electricity carbon intensity in European member states: impacts on GHG emissions of electric vehicles. Transport. Res. Part D 64, 5–14. https://doi.org/10.1016/j.trd.2017.07.012.

Nemhauser, G.L., Wolsey, L.A., 1988. Integer and Combinatorial Optimization. John Wiley & Sons, United States of America.

Nguyen, T., Abdin, Z., Holm, T., Mérida, W., 2019. Grid-connected hydrogen production via large-scale water electrolysis. Energy Convers. Manag. 200, 112108. https://doi.org/10.1016/j.enconman.2019.112108.

Norgate, T., Haque, N., 2010. Energy and greenhouse gas impacts of mining and mineral processing operations. J. Clean. Prod. 18, 266–274. https://doi.org/10.1016/j.jclepro.2009.09.020.

Otto, A., Robinius, M., Grube, T., Schiebahn, S., Praktiknjo, A., Stolten, D., 2017. Power-to-steel: reducing CO2 through the integration of renewable energy and hydrogen into the German steel industry. Energies 10, 451–471. https://doi.org/10.3390/en10040451.

Pardo, N., Moya, J.A., 2013. Prospective scenarios on energy efficiency and CO2 emissions in the European iron & steel industry. Energy 54, 113–128. https://doi.org/10.1016/j.energy.2013.03.015.

Pardo, N., Moya, J.A., Vatopoulos, K., 2012. Prospective Scenarios on Energy Efficiency and CO2 Emissions in the EU Iron & Steel Industry. European Commission - Joint Research Centre - Institute for Energy and Transport. https://doi.org/10.2790/64264. Report.

Parra, D., Valverde, L., Pino, F.J., Patel, M.K., 2019. A review on the role, cost and value of hydrogen energy systems for deep decarbonisation. Renew. Sustain. Energy Rev. 101, 279–294. https://doi.org/10.1016/j.rser.2018.11.010.

Parra, D., Zhang, X., Bauer, C., Patel, M.K., 2017. An integrated techno-economic and life cycle environmental assessment of power-to-gas systems. Appl. Energy 193,

440–454. https://doi.org/10.1016/j.apenergy.2017.02.063.

Parra De Lazzari, C., Capocchi, J.D.T., 1997. Copper deoxidation by bubbling hydrogen/nitrogen mixtures through the melt. In: Mishra, B. (Ed.), EPD Congress 1997: Proceedings of Sessions and Symposia Sponsored by the Extraction and Processing Division, Orlando, Florida, USA, 9-13 February 1997, the Minerals. Metals & Materials Society.

Proost, J., 2019. State-of-the art CAPEX data for water electrolysers, and their impact on renewable hydrogen price settings. Int. J. Hydrogen Energy 44, 4406–4413. https://doi.org/10.1016/j.ijhydene.2018.07.164.

Qu, G., Wei, Y., Li, B., Wang, H., Yang, Y., McLean, A., 2020. Distribution of copper and iron components with hydrogen reduction of copper slag. J. Alloys Compd. 824, 153910. https://doi.org/10.1016/j.jallcom.2020.153910.

Ramachandran, V., Díaz, C., Eltringham, T., Lehner, T., Mackey, P.J., Newman, C.J., Tarasov, A., 2003. Primary copper production - a survey of operating world copper smelters. In: Díaz, C., Kapusta, J., Newman, C. (Eds.), Proceedings of the Copper 2003-Cobre 2003, the 5th International Conference, Volume IV — Pyrometallurgy of Copper (Book 1), the Hermann Schwarze Symposium on Pyrometallurgy, Santiago, Chile, 30 November - 3 December 2003. Canadian Institute of Mining, Metallurgy and Petroleum, pp. 3–106.

Reuter, M.A., van Schaik, A., Gediga, J., 2015. Simulation-based design for resource efficiency of metal production and recycling systems: cases - copper production and recycling, e-waste (LED lamps) and nickel pig iron. Int. J. Life Cycle Assess. 20, 671–693. https://doi.org/10.1007/s11367-015-0860-4.

Reuter, M.A., van Schaik, A., Gutzmer, J., Bartie, N., Abadías-Llamas, A., 2019. Challenges of the circular economy: a material, metallurgical, and product design perspective. Annu. Rev. Mater. Res. 49, 253–274. https://doi.org/10.1146/annurev-matsci-070218-010057.

Rogelj, J., Shindell, D., Jiang, K., Fifita, S., Forster, P., Ginzburg, V., Handa, C., Kheshgi, H., Kobayashi, S., Kriegler, E., Mundaca, L., Séférian, R., Vilariño, M.V., 2018. Mitigation pathways compatible with 1.5°C in the context of sustainable development. In: Masson-Delmotte, V., Zhai, P., Pörtner, H.O., Roberts, D., Skea, J., Shukla, P.R., Pirani, A., Moufouma-Okia, W., Pèan, C., Pidcock, R., Connors, S., Matthews, J.B.R., Chen, Y., Zhou, X., Gormis, M.I., Lonnoy, E., Maycock, T., Tignor, M., Waterfield, T. (Eds.), Global Warming of 1.5°C an IPCC Special Report on the Impacts of Global Warming of 1.5°C above Pre-industrial Levels and Related Global Greenhouse Gas Emission Pathways, in the Context of Strengthening the Global Response to the Threat of Climate Change, Sustainable Development, and Efforts to Eradicate Poverty. Intergovernmental Panel on Climate Change.

Rosenfeld, D.C., Böhm, H., Lindorfer, J., Lehner, M., 2020. Scenario analysis of implementing a power-to-gas and biomass gasification system in an integrated steel plant: a techno-economic and environmental study. Renew. Energy 147, 1511–1524. https://doi.org/10.1016/j.renene.2019.09.053.

Sallee, J.E., Ushakov, V., 1999. Electric settling furnace operations at the Cyprus Miami Mining Corporation copper smelter. In: George, D.B., Chen, W.J., Mackey, P.J., Weddick, A.J. (Eds.), Copper 99-Cobre 99, pp. 629–644.

Schlesinger, M.E., King, M.J., Sole, K.C., Davenport, W.G., 2011. In: Extractive Metallurgy of Copper, fifth ed. Elsevier. https://doi.org/10.1016/C2010-0-64841-3.

Segura-Salazar, J., Lima, F.M., Tavares, L.M., 2019. Life cycle assessment in the minerals industry: current practice, harmonization efforts, and potential improvement through the integration with process simulation. J. Clean. Prod. 232, 174–192. https://doi.org/10.1016/j.jclepro.2018.05.318.

Siemens, AG, 2018. SILYZER 300. Die nächste Dimension der PEM Elektrolyse. Report. Siemens AG. https://new.siemens.com/global/de/produkte/energie/erneuerbare-energien/hydrogen-solutions.html#Portfolio. Accessed: 2019-04-30.

Smolinka, T., Wiebe, N., Sterchele, P., Palzer, A., Lehner, F., Jansen, M., Kiemel, S., Miehe, R., Wahren, S., Zimmermann, F., 2018. Studie IndWEDe - Industrialisierung der Wasserelektrolyse in Deutschland: Chancen und Herausforderungen für nachhaltigen Wasserstoff für Verkehr, Strom und Wärme. Report. NOW-GmbH. Berlin. http://publica.fraunhofer.de/documents/N-519494.html. Accessed: 2019-12-16.

Song, X., Pettersen, J.B., Pedersen, K.B., Røberg, S., 2017. Comparative life cycle assessment of tailings management and energy scenarios for a copper ore mine: a case study in northern Norway. J. Clean. Prod. 164, 892–904. https://doi.org/10.1016/j.jclepro.2017.07.021.

Soulier, M., Pfaff, M., Goldmann, D., Walz, R., Geng, Y., Zhang, L., Tercero Espinoza, L.A., 2018. The Chinese copper cycle: tracing copper through the economy with dynamic substance flow and input-output analysis. J. Clean. Prod. 195, 435–447. https://doi.org/10.1016/j.jclepro.2018.04.243.

Steelonthenet, 2019. European met coke prices. https://www.steelonthenet.com/files/blast-furnace-coke.html/. Accessed: 2020-04-14.

Sunfire GmbH, 2020. Sunfire-hylink factsheet. https://www.sunfire.de/files/sunfire/images/content/Produkte_Technologie/factsheets/Sunfire-HyLink_FactSheet.pdf. Accessed: 2020-03-18.

Suopajärvi, H., Umeki, K., Mousa, E., Hedayati, A., Romar, H., Kemppainen, A., Wang, C., Phounglamcheik, A., Tuomikoski, S., Norberg, N., Andefors, A., Öhman, M., Lassi, U., Fabritius, T., 2018. Use of biomass in integrated steelmaking — status quo, future needs and comparison to other low-CO2 steel production technologies. Appl. Energy 213, 384–407. https://doi.org/10.1016/j.apenergy.2018.01.060.

Thema, M., Bauer, F., Sterner, M., 2019. Power-to-gas: electrolysis and methanation status review. Renew. Sustain. Energy Rev. 112, 775–787. https://doi.org/10.1016/j.rser.2019.06.030.

Thyssenkrupp, 2019. World first in Duisburg as NRW economics minister Pinkwart

launches tests at thyssenkrupp into blast furnace use of hydrogen. https://www.thyssenkrupp-steel.com/en/newsroom/press-releases/world-first-in-duisburg.html. Accessed: 2019-12-18.

Van der Voet, E., Van Oers, L., Verboon, M., Kuipers, K., 2018. Environmental implications of future demand scenarios for metals: Methodology and application to the case of seven major metals. J. Ind. Ecol. 23, 141–155. https://doi.org/10.1111/jiec.12722.

Voll, P., Klaffke, C., Hennen, M., Bardow, A., 2013. Automated superstructure-based synthesis and optimization of distributed energy supply systems. Energy 50, 374–388. https://doi.org/10.1016/j.energy.2012.10.045.

Wang, S., Davenport, W., Yao, S., Walters, G., Gonzales, T., Siegmund, A., George, D.B., 2019. Copper smelting: 2019 world copper smelter data. In: Proceedings of the 58th Annual Conference of Metallurgists (COM) Hosting the 10th International Copper Conference 2019. Canada, Vancouver, pp. 18–21. August 2019.

Warczok, A., Riveros, G., 2007. Slag cleaning in crossed electric and magnetic fields.

Miner. Eng. 20, 34–43. https://doi.org/10.1016/j.mineng.2006.04.007.

Weigel, M., Fischedick, M., Marzinkowski, J., Winzer, P., 2016. Multicriteria analysis of primary steelmaking technologies. J. Clean. Prod. 112, 1064–1076. https://doi.org/10.1016/j.jclepro.2015.07.132.

Wietschel, M., Kühnbach, M., Rüdiger, D., 2019. Die aktuelle Treibhausgase-missionsbilanz von Elektrofahrzeugen in Deutschland. Report working paper on sustainability and innovation No. S 02/2019. Fraunhofer ISI. http://publica.fraunhofer.de/documents/N-537432.html. Accessed: 2020-11-03.

Zhang, W., Li, Z., Dong, S., Qian, P., Ye, S., Hu, S., Xia, B., Wang, C., 2021. Analyzing the environmental impact of copper-based mixed waste recycling-a LCA case study in China. J. Clean. Prod. 284, 125256. https://doi.org/10.1016/j.jclepro.2020.125256.

Zhang, X., Bauer, C., Mutel, C.L., Volkart, K., 2017. Life cycle assessment of power-to-gas: approaches, system variations and their environmental implications. Appl. Energy 190, 326–338. https://doi.org/10.1016/j.apenergy.2016.12.098.